Journal of Alloys and Compounds 849 (2020) 156718

Contents lists available at ScienceDirect

Journal of Alloys and Compounds

journal homepage: http://www.elsevier.com/locate/jalcom

Physical and optical studies of the novel non-crystalline $Cu_xGe_{20-x}Se_{40}Te_{40}$ bulk glasses and thin films

Ahmed Saeed Hassanien [a, b, 1, *], I.M. El Radaf [c, d], Alaa A. Akl [e, f]

[a] Engineering Math. and Physics Department, Faculty of Engineering (Shoubra), Benha University, 11629, Egypt
[b] Physics Department, Faculty of Science and Humanities in Afif Governorate, Shaqra University, 11921, Saudi Arabia
[c] Physics Division, Electron Microscope and Thin Films Dept, National Research Centre, Dokki, Giza, 12622, Egypt
[d] Materials Physics and Energy Laboratory, College of Sciences and Art at Ar-Rass, Qassim University, 51921, Saudi Arabia
[e] Physics Department, Faculty of Science, Minia University, 111955, Egypt
[f] Physics Department, Faculty of Science and Humanities in Ad-Dawadmi Governorate, Shaqra University, 11911, Saudi Arabia

ARTICLE INFO

Article history:
Received 13 February 2020
Received in revised form
18 July 2020
Accepted 13 August 2020
Available online 16 August 2020

Keywords:
Glassy bulk samples
Physical deposition technique
Amorphous thin films
Optical properties
Chemical bond approach
Cohesive energy

ABSTRACT

In this research work, the authors devoted their efforts to study the physical and optical properties of the novel $Cu_xGe_{20-x}Se_{40}Te_{40}$, CGST (x = 0,5,10,15,20 at.%) matrix. Physical properties of bulk samples and optical properties of thin films of this matrix have been studied. The bulk glassy samples were prepared using the known melt quenching method, while thin-film samples were deposited by vacuum deposition technique under pressure 10^{-4} Pa. X-ray diffraction examination showed that thin-film samples were deposited in the amorphous state, where no discrete sharp diffraction peaks were formed. Energy-dispersive X-ray spectroscopy exhibited also that there is a good agreement between the experimental results and the selected elemental composition ratios for all samples. The optical properties were studied using the spectrophotometric measurements of transmittance and reflectance spectra within the spectral range 300 nm–2500 nm. The absorption coefficient, the absorption index, optical energy gap, Urbach energy and others have been investigated and discussed on the view of the chemical band approach model. The optical energy gap decreases from 1.208 eV to 1.045 eV, while Urbach energy increases from 0.186 eV to 0.219 eV as Cu ratio increased from zero to 20%. These CGST samples showed very low absorbance nature in the NIR and IR regions. Therefore, they can be used in the applications of opto-electronics devices, infrared imaging, and optical filters and detectors.

1. Introduction

In the past few decades, chalcogenide glassy compositions and/or alloys containing transitional metal have become more attractive materials for researchers. The most common chalcogenide semiconductor structures are those belonging to I-IV-VI compositions, such as those consists of Cu or Ag, group (I), Ge or Si, group (IV) and S, Se and/or Te from the group (VI). This is owing to their distinguishing, convenient and unique physical properties, e.g., good chemical stability, a high index of refraction, quantum detectors, stronger photosensitivity, high transparency in the infrared, IR region [1–3]. Consequently, they have wide potential applications in several electronics industries. Whereas, these materials are used in many implementations, like a thin film transistor, waveguides, optical fibers, optoelectronic, photo-voltaic, solid-state devices, memory components and nonlinear optics [4–6]. Further, most of the I-IV-VI compositions are good absorbing materials, so they widely used in the solar photovoltaic cells [7,8]. The reason that led to the widespread usage of such materials is also the ability to control or modify their physical properties, even after their synthesis. Where the properties of the chalcogenide materials can also be controlled by influencing upon the sample with external effects (such as effecting on the sample by Gamma rays, Laser beams, the thermal treatment processes, the scale of Tera watt, STW renewable energy generation, …and others), which lead to improve their properties, as well as can modify the properties of the sample as

* Corresponding author. Engineering Math. and Physics Department, Faculty of Engineering (Shoubra), Benha University, 11629, Egypt.
E-mail addresses: a.s.hassanien@gmail.com, ahmed.hassanien@feng.bu.edu.eg (A.S. Hassanien).
[1] Permanent address of the corresponding author (Ahmed Saeed Hassanien) is: mailto:ahmed.hassanien@feng.bu.edu.eg Engineering Math. and Physics Department, Faculty of Engineering at Shoubra, 11629, Benha University, Egypt.

https://doi.org/10.1016/j.jallcom.2020.156718
0925-8388/

required and according to the application in which they can be employed [3-8].

On the other hand, chalcogenide, ChG alloys and compositions are considered from the most famous categories of amorphous materials [9,10]. While the ternary Ge—Se—Te glasses and their film samples are the most common non-crystalline chalcogenides. Generally, ChG and their films are promising optical substances owing to their transparency nature in the infrared region, they are non-dispersed materials, of lower optical losses, and have good chemical and mechanical properties [11–15]. Therefore, ChG materials, whether bulk or thin-film samples, are a candidate for many technological and scientific applications and devices, especially in the fabrication of transparent thermal-imaging lenses and sensors in the infrared region, as well as, the optical glass fibers [15–17]. Therefore, they have received great attention and attract many scholars to research in. Therefore, the authors and their colleagues carried out a thorough study of a-$Ge_{10+x}Se_{40}$—Te_{50-x} samples, where they studied the optical, electrical and thermal characteristics of these amorphous samples [18–20]. Moreover, the authors also extensively discuss many of optical and physical properties of the quaternary a-Ge-Sb-Se-Te bulk glasses and their thin-film specimens [21–23]. In addition, they studied the effect of Cu-addition on the structural, optical and optoelectrical properties of many other compositions, like Cu_2MnGeS_4, Cu_2MnSnS_4 and $Cu_2ZnGeSe_4$ [24–27]. Therefore, the authors have decided to synthesize and study the physical and optical properties of the novel quaternary a-Cu-Ge-Se-Te bulk and film samples, in the current article.

The addition of the copper leads to the enhancement and strengthen the glass structure of the composition, as proposed by Barisova [28]. Furthermore, the addition of more copper to chalcogenide compositions, with a maximum of 20% of the atomic weight of the constituents of that composition [16,28,29], leads to improve their optical and physical properties [30]. Moreover, the Cu—addition will result in a decrease in the band-gap energy, E_g, thereby decreases the conductivity activation energy, ΔEE of these systems. Besides, these copper-chalcogenide structures will also possess new attractive properties such as flexibility, high strength, high optical reflectance and high optical recording materials along with the development of some other individual abilities [9,10,30,31]. Thus, these glasses can be used to produce many electronic components, especially those that need the existence of metals [10]. Moreover, they are extensively used in our daily lives; like light bulbs, optical windows, displays and optical fibers, and even they have employed as architecture constructing materials [31,32]. On the other hand, almost all Cu-ChG thin films can be synthesized by physical vapor deposition, PVD [9,10,16,29–33]. This vapor deposition technique is one of the most accurate methods used to prepare the film samples. It is distinguished from other preparation methods of film samples, where all experimental conditions of depositing films can be controlled in, like the deposition rate, evaporation period and thickness of the film, besides, the structure and morphology of deposit films [5,7,34].

This research aims to synthesize glassy bulk and thin-film samples of the novel $Cu_xGe_{20-x}Se_{40}Te_{40}$ glassy compositions ($0.00 \leq x \leq 20.00$, at. %) with high quality and homogenity. Besides, the authors have aim also to discuss the effect of replacing Cu instead of Ge within the non-crystalline Cu-Ge-Se-Te matrix. In addition, to investigate such replacement upon the physical and optical characteristics of these chalcogenide $Cu_xGe20\text{-}_xSe_{40}Te_{40}$ samples. The goal of this work is the study and discuss the mass-volume density and some important related physical factors, like molar volume, percentage of the free volume, compactness, packing density and many others. The atomic density and its related parameters are also aiming to be investigated. The optical properties of these novel systems are aimed to be studied. Table 1 summarizes some important characterizations of the raw starting materials used. It includes the values of the following; the density, $\rho_{element}$, molar volume, V_M, molar mass, M_M, atomic density, AD, electro-negativity, EN, band-gap energy, E_g, bond energy, BE, co-ordination number of element, $<N_c>$, ionization energy, E^M_{Ion}, electron-affinity, E^M_{Aff} and the heat of atomization, H_s [35–38].

2. Materials and experimental procedures

2.1. Synthesis of bulk and film samples

Elemental powders of copper, germanium, selenium, and tellurium of high purity degrees have been employed to synthesize the amorphous samples of the $Cu_xGe_{20-x}Se_{40}$-Te_{40} system. The purity degree of these elements was greater than or equal 4 N and they were purchased from Sigma – Aldrich company. Appropriately selected proportions from the power of the elements were weighted in accordance with the atomic weights of the constituents of the matrix. The mixtures were placed in quartz tubes and then sealed under vacuum. Where the tubes were evacuated to about 10^{-3} Pa. These evacuated tubes were placed in a rocking-electric oven and then it gradually was heated. The heating process was carried out initiating from the room temperature up to 1300 K, under the heating rate 3–4 K/min. Moreover, the tubes were left within the furnace for 24 h at this final temperature degree (1300 K) to warranty the best mixing and homogeneity of the molten CGST alloys. After this, the tubes and their molten compositions were suddenly quenched in ice-water to get the quaternary non-crystalline Cu-Ge-Se-Te alloys. Then, the quartz tubes were broken to get their ingots, which were used to prepare thin-film samples of these $Cu_xGe_{20-x}Se_{40}$-Te_{40} synthesized compositions. Thin films have been deposited by the physical evaporation deposition method by using the coating unit of Edward - model (E 306A) [39,40].

There were some preparatory conditions that were taken into account and applied to obtain high-quality and homogenous thin films; these conditions were: (i) The pressure within the coating unit was about 10^{-4} Pa. (ii) The distance between the molybdenum boat and the substrate was controlled to get uniform film of constant thickness. (iii) The glass substrates used in this research work were microscopic glass sheets known as “KH-Glass Microscopic slides” of high optical transparency. Their dimensions are 76.2 × 25.4 Sq. mm (about 3 × 1 $inch^2$) and of thickness about 1.0 mm [26]. These glass sheets have a high optical quality, where they depicted by their free of inclusions and bubbles, high purity, clearness and colorlessness [41]. (iv) The surfaces of the used glass substrate have been well pre-cleaned before the deposition process of the thin film. The substrate surfaces well washed with detergent and water, followed by acetone for 5 min. Then, rinse with de-ionized water, and then ultrasound cleaned. Finally dried by hot air and then have been fixed in its holder within the vacuum jar [26]. It is worth mentioning that the material of the substrate surface plays a substantial role in the morphology of the deposited thin-film samples. Practically, the thin-film morphology is strongly dependent on the crystal structure and morphology of the used substrate. If the material of the substrate surface is very crystallized, like silicon dioxide, it assists to increase the crystallization of the film and vice versa. The crystal structure of the first layers adjacent to the surface of the substrate depends on its growth on the direction of crystallization on the substrate surface. But if the material of the surface of the substrate has a non-crystalline nature, as the present case, then the first layers adjacent to the surface of the substrate will have the same non-crystallinity form [25,26]. (v) The

Table 1
The most important factors of used raw elements of a-Cu_x Ge_{20-x} Se_{40} Te_{40} samples [35–38].

Element	$\rho_{element}$ (gm/cm^3)	V_M (cm^3/mol)	M_M (gm/mol)	AD × 10^{22} (atoms/cm^3)	EN (Pauling scale)	E_g (eV)	BE (eV)	N_C	E^M_{Ion} (eV)	E^M_{Aff} (eV)	H_s kCal/g.atom
Cu	*8.92*	*7.11*	*63.55*	*8.471*	*1.90*	*——*	*7.659*	*1*	*7.726*	*1.229*	*81.1*
Ge	*5.32*	*13.63*	*72.63*	*4.419*	*2.01*	*0.67*	*7.889*	*4*	*9.899*	*1.235*	*90.0*
Se	*4.97*	*16.42*	*78.97*	*3.668*	*2.55*	*1.74*	*6.448*	*2*	*9.767*	*2.023*	*49,4*
Te	*6.24*	*20.46*	*127.60*	*2.944*	*2.10*	*0.34*	*6.001*	*2*	*9.020*	*1.974*	*46.0*

deposition rate was adjusted to be 10 nm/s (vi) The deposition time was about 25 s (vii) The thickness monitor was controlled to get film samples have a thickness equal 200 nm. Where, the quartz crystal oscillator (Edwards of the model FTM-3) was located very close to the glass substrate. Finally, (viii) synthesized film samples were preserved within the chamber of the coating unit for about 24 h to realize the equilibrium metastable state [34]. Thereby, these procedures lead to obtaining high-quality film samples, where they will have a uniform thickness, smooth surface, and tightly sticking to the substrate [9,21,30].

2.2. Used characterization techniques

The amorphous and/or crystalline nature of $Cu_xGe_{20-x}Se_{40}Te_{40}$ bulk and film samples were examined using X-ray diffraction. The used diffractometer in this work was JEOL of the model JSDX- 60-PA. It should note that to get accurate structural results, it was used a high-energy power source of 35 mA and 40 kV. Furthermore, a very low continuous scanning rate, 0.02 °/s was applied, as it was achieved, here, to detect any probable diffraction lines or any formed or separated phases that may be found. It is worthy to mention that the sample examination via XRD is not a suitable method only, but it is a very good technique to judge the structural nature of the samples. Further, it is an easy, very reliable and cheap technique. The used radiation source was Cu-k_α of wavelength about 1.54184 Å, and of an energy about 8.042 KeV. The samples were scanned at room temperature in the range between 10° and 80° of the diffraction angles. On the other hand, the synthetic compositional element ratios of the prepared samples were analyzed using the energy-dispersive X-ray spectroscopy analysis, EDS technique. This EDS unit was attached to a scanning electron microscope, SEM, then it was operated with 30 kV accelerating voltage. The measured compositional element ratios of the Cu-Ge-Se-Te system were checked several times at different places and the average values were considered. All EDS-images were scanned at room temperature. The error recorded in the EDS obtained results was very minimal; it did not exceed ±1.00%.

The mass-volumetric density, ρ_S^{exp} – values of the bulk samples of the current glasses were determined by using Archimedes' Principle, using a non-solvent (toluene) liquid, which was used as a buoyant liquid. The measured values were recorded at room temperature. The experiment was performed many times and the mean value for each sample was taken. The error of in determining the density values was within ±1.30%.

Optical properties of chalcogenide $Cu_xGe_{20-x}Se_{40}$-Te_{40} amorphous films were achieved via the measurements of both the transmittance, T and reflectance, R, of samples in the range 300 nm–2500 nm of wavelength. A double beam UV-Vis-NIR-Shimadzu spectrophotometer of the model UV-310-PC was used to record both the T - and R - Spectra. This spectrophotometer is equipped with a reflection attachment to measure the reflectivity of samples, it is of the V–N type (angle of incidence is 5°). The absorption coefficient, α of film samples has been calculated from the corrected values of both T and R measurements. The error value in the determination of the absorption coefficient, α-spectra of the quaternary Cu-Ge-Se-Te film samples was about ±0.85%. All discussed optical properties were investigated at room temperature.

3. Theoretical considerations and used equations

3.1. Density and its related parameters

The density of any substance can be measured using Archimedes' principle using a non-solvent liquid (toluene), used as a buoyant liquid. The density of can be determined from the following Eq.: $= \rho_S^{exp} = \rho_{BL}\left(\frac{W_a}{\Delta W}\right)$.

Where, ρ_{BL} is the density of the buoyant liquid [42–44]. While, ΔW is the weight of a bulk sample in air, W_a minus its weight in the buoyant liquid, W_{BL}, i.e. $\Delta W = W_a - W_{BL}$. Therefore, the molar volume, V_M of the sample can be obtained using this form $V_M = \frac{1}{\rho_S^{exp}} \sum x_i M_m$.

Where, ρ_S^{exp} is the measured density, while $\sum x_i M_m$ is the molar mass of the sample, which can be determined from this form [45]: $\sum x_i M_m = (\alpha\, Mm)_{Cu} + (\beta\, Mm)_{Ge} + (\gamma\, Mm)_{Se} + (\delta\, Mm)_{Te}$.

Here, α, β, γ and δ are the fraction percent of Cu-, Ge-, Se- and Te-elements. The excess volume V_e is the difference between the experimentally measured and theoretically calculated molar volumes, V_M *and* V^{th}, respectively, i.e., $V_e = V_M - V^{th}$, noting that $V^{th} = \sum_i x_i\, V_M(i)$, here $V_M\,(i)$ is the molar volume of each element.

The theoretical molar volume, V^{th} is also calculated from this Eq. [45]:

$$\boldsymbol{V^{th} = \alpha V_M(Cu) + \beta V_M(Ge) + \gamma\, V_M(Se) + \delta V_M\,(Te)} \quad (1)$$

There is a difference between the theoretical and experimental values of the molar volume. So, there is the free volume percentage, *FVP*, which can be computed as follows: $FVP = \frac{V_M - V^{th}}{V_M} \times 100\%$ [45,46].

The packing density, D_p of a sample is the fraction of the space that is filled with the elements making up the lattice, it is sometimes called the packing fraction. It also specifies the ratio of the used space to a selected one, is given by this Eq. [45,47]:

$$D_P = \frac{\boldsymbol{\rho_S^{exp}} \times \boldsymbol{N_A}}{\boldsymbol{M_m}} = \frac{\boldsymbol{N_A}}{\boldsymbol{V_M}} \quad (2)$$

where, N_A is Avogadro's number and V_M is the molar volume of the sample, ρ_S^{exp} is the experimental density value and M_m is the sample molar volume. On the other hand, the compactness parameter, δ can be obtained by using this Eq. [42,48]:

$$\boldsymbol{\delta} = \left[\frac{\sum_i \frac{x_i (M_m)_i}{\rho_i} - \sum_i \frac{x_i (M_m)_i}{\rho}}{\sum_i \frac{x_i (M_m)_i}{\rho}}\right] \quad (3)$$

where, the symbol (x_i) refers to the molar ratio % of elements, which

participate in the CGST glassy compositions. While, the parameter $(M_m)_i$ is the molar mass of that composition and ρ_i is the density of each element, while ρ is the atomic density of the studied composition.

Moreover, using Naster–Kingery formula of the atomic density, *AD*, it can estimate the values of this parameter for the current elements existing in the Cu-Ge-Se-Te bulk glassy alloys. This form is given as follows [42,49]: $AD = \frac{\rho_S^{exp} \times W_p \times N_A}{AW \times 100}$.

Where ρ_s is the sample density, N_A is Avogadro's number, W_P is the element percentage in its composition (atomic fraction), *AW* is the ratio between the molar mass (atomic weight) of the element and the molar mass of its composition. Further, if the value of the *AD* parameter is known, anyone can get the interatomic, $IAS_{Atom-Atom}$. This parameter can be evaluated from this simple Eq. [50]: $IAS_{Atom-Atom} = (1/AD)^{1/3}$. Moreover, by knowing the distance, $IAS_{Atom-Atom}$, it can evaluate the polaron radius, R_p from this simple Eq.:

$$\boldsymbol{R_p} = \frac{1}{2}\left(\frac{\pi}{6\,\boldsymbol{AD}}\right)^{1/3} = \left(\frac{\pi}{48\,\boldsymbol{AD}}\right)^{1/3} = \boldsymbol{\eta \times IAS_{Atom-Atom}} \tag{4}$$

where, η is a dimensionless constant ($\eta = 0.403$), Hence, the field strength, *FS*, which is the strength of the atomic field of a certain atom, can be calculated by knowing the number of valence electron, $V_{No.}$ of the atom and the corresponding polaron radius, R_p as follows.: $FS = \left(\frac{V_{No.}}{R_p^2}\right)$ [49,50].

3.2. Bandgap energy, the cohesive energy and coordination number

Shimakawa assumed that the energy bandgap of any semiconductor composition or alloy consists of multi-elements can be theoretically calculated if the value of the band gap energies of the constituent elements of that composition or alloy are known. He argued that the bandgap-energy value, E_g^{th} can be computed by this Eq. [51,52]:

$$\boldsymbol{E_g^{th}} = \sum_i \boldsymbol{x E_{g_{(element)}}} = \boldsymbol{\alpha E_{g(A)} + \beta E_{g(B)} + \gamma E_{g(C)} + \delta E_{g(D)}} \tag{5}$$

where, α, β, γ and δ are the atomic fractions, while $E_{g(A)}$, $E_{g(B)}$, $E_{g(C)}$ and $E_{g(D)}$ are the bandgap-energy values of the elements A, B, C and D, respectively; the value of those energies was reported in Table 1. On the other hand, the cohesive-energy value, E_C can be calculated on the bases of the chemical bond approach model, CBA as follows [34,53,54]: $\boldsymbol{E_C} = \sum_i \left(\frac{\boldsymbol{NE_B}}{100}\right)_i$.

Where, N_i is the number of chemical bonds expected to form between any two atoms of the elements of that composition. While, E_{B_i} is the energy value of the chemical bond, which expect to be formed. The bond formed between two atoms belonging to the same element is a weak bond; it is called a homonuclear (homopolar) bond. This type of bond is considered a defect bond. While, the heteronuclear (heteropolar) bond, which is the strongest and preferred bond between any two atoms belong to two different elements.

The energy of the heteronuclear bond can be computed by knowing the heteronuclear bond energy of the two elements and the electro-negativity values, χ_A and χ_B of these two elements by using the following form [55–57]:

$$\boldsymbol{E_B(A-B)} = [\boldsymbol{E_B(A-A)} \times \boldsymbol{E_B(B-B)}]^{1/2} + 30(\chi_A - \chi_B)^2 \tag{6}$$

Besides, the number of atoms of the nearest neighbor which is called the number of the average coordination, is denoted as N_C and can be determined for amorphous materials, knowing both the atomic fractions, $(\alpha, \beta, \gamma \text{ and } \delta)$ and the number of valence electrons, $VE_{No.}$ of the participated chemical elements which constitute of the CGST matrix, from the following Eq. [34,58]:

$$\boldsymbol{N_C} = \left(\frac{\boldsymbol{\alpha VE_{No.A} + \beta VE_{No.B} + \gamma VE_{No.C} + \delta VE_{No.D}}}{\boldsymbol{\alpha + \beta + \gamma + \delta}}\right) = \left(\frac{\boldsymbol{\alpha\ VE_{No.A} + \beta\ VE_{No.B} + \gamma\ VE_{No.C} + \delta\ VE_{No.D}}}{100}\right) \tag{7}$$

The lone-pair electrons, *LP* of any bulk glassy composition can be calculated if the values of both the number of valence electrons, $V_{No.}$ and N_C using this direct formula [59–61]: $\boldsymbol{LP} = \boldsymbol{VE_{No.}} - \boldsymbol{N_C}$. The floppy modes, *FM* of any bulk glassy alloy, which indicates if the sample lies or not in the floppy region, can be calculated from this Eq. [42,45]: $\boldsymbol{FM} = 2 - \frac{5\,\boldsymbol{N_C}}{6}$.

On the other hand, the total number of mechanical bond constraints, NTotal con of any glassy system is originated from two types of constraints; they are the bond bending and the bond stretching constraints (N_{bb} and N_{bs}, respectively). Therefore, the total number of the bond constraints is given as [45,48,62]:

$$\boldsymbol{N_{Total\ Cont.}} = \boldsymbol{N_{bb} + N_{bs}} = \frac{5\boldsymbol{N_C}}{2} - 3 \tag{8a}$$

$$\text{Where } \boldsymbol{N_{bb}} = \frac{1}{2}\,\boldsymbol{N_C} \text{ and } \boldsymbol{N_{bs}} = [2\boldsymbol{N_C} - 3] \tag{8b}$$

The value of the density of the cross-linking, D_{CL} and the effective coordination number, $N_{C_{Eff}}$ can also be determined from the obtained values of the total number of constraints, NTotal con, as follows [45,62].

$$\boldsymbol{D_{CL}} = \boldsymbol{N_{Total\ Cont.}} - 2 \text{ and } \boldsymbol{N_{C_{Eff}}} = \frac{2}{5}\boldsymbol{N_{Total\ Cont.}} + 3 \tag{8c}$$

4. Results and discussion

4.1. Identification of a-CGST thin-film samples

The crystalline/non-crystalline nature of the new quaternary $Cu_xGe_{20-x}Se_{40}Te_{40}$, CGST bulk alloy samples were examined by the X-ray diffraction technique, XRD. The X-ray diffractograms showed that the synthesized quenched bulk samples for all atomic fractional ratios ($0 \le x \le 20$ at. %) are free of either the discrete or sharp diffraction peaks. This means that these ingots bulk samples have the amorphous nature. Furthermore, when examining the deposited films of this novel Cu-Ge-Se-Te system, it was also found that there are no sharp or discrete diffraction lines, at all, as depicted in Fig. (1). This affirms that all Cu-Ge-Se-Te samples have been deposited in the amorphous phase. It is worthy to note from Fig. (1) that these diffractograms show common behavior and all of them have a broad stepped hump. This hump is located between the two diffraction angles (2θ) 20° and 40°. This behavior was popular and reported for many non-crystalline film samples [18,21,22].

On the other hand, the atomic ratios of the compositional elements of the as-deposited quaternary Cu_{20} $Se_{40}Te_{40}$ films have checked by the energy-dispersive X-ray spectroscopy, EDS to confirm the elemental ratios of each sample. It is worth mentioning also that the process of scanning has been done at the film's surface several times for each sample, to confirm the correctness of the obtained distribution ratios of the elements of each sample [41,63,64]. It was observed that the distribution of the atomic ratios

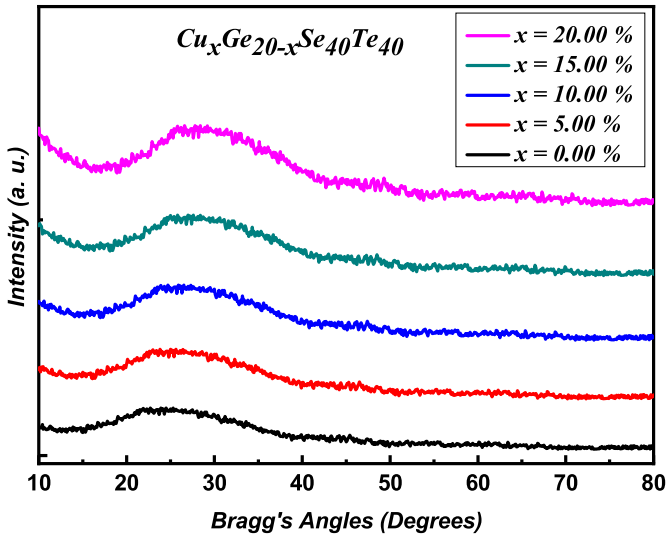

Fig. 1. XRD patterns of the novel quaternary a-Cu-Ge-Se-Te thin films.

of films is in a good matching with the selected ones. Table 2 reports a comparison between the obtained experimental EDS results and those were selected and based on them the samples were prepared. It is worth noting that the experimental error is less than ± 1.00%.

4.2. Density and some concerned parameters

The density, ρ_S^{exp} of the novel Cu_x Ge_{20-x} Se_{40} Te_{40} bulk samples have been experimentally measured using the Archimedes' method, where the employed buoyant liquid was the toluene. The measurements were repeated three times and the average values were considered. The values of the density were found to increase as the ratio of the copper was increased. The obtained experimental results were listed in Table 3 and then illustrated as a function of Cu-content percent (x) in Fig. (2-a). This figure was fitted to get a linear relationship between ρ_S^{exp} and (x) and the empirical equation that describes this direct proportion can be expressed as: $\boldsymbol{\rho_S^{exp}(g/cm^3) = 5.325 + 0.027\ x,}$

Where, x is the molar fraction percentage of the Cu. The increasing values of ρ_S^{exp} of Cu-Ge-Se-Te samples can be attributed to the density values of Cu and Ge. Where, Cu increased in the account of Ge, and at the same time the density of Cu, ρ_{Cu} = 8.92 (g/cm^3) is larger than that of the Ge, ρ_{Ge} = 5.32 (g/cm^3), as reported in Table 1.

On the other hand, the density values of all prepared bulk samples were theoretically computed and reported also in Table 3. The authors have used the empirical form that proposed by Fayek et al. [13]. This experimental expression is given as follows: $\boldsymbol{\rho_S^{Th}} = \sum \left(\frac{P_i}{d_i}\right)^{-1}$,

where P is the elemental molar fraction of each participating element and d is the density of each separate element [13]. If anyone compares experimental and theoretical density values, he can find that there is a good agreement between the two obtained values. Depending on the determined experimental-density values of the Cu-Ge-Se-Te bulk samples, the molar volume, V_M can be computed. The estimated V_M-values were tabulated also in Table 3 and plotted as a function of the molar fraction of the Cu-content (x), as shown in Fig. (2-b). The graph is also fitted to obtain a straight line, as shown. The experimental equation for the straight line shown is given by the following Eq.: $\boldsymbol{V_M\ (cm^3/mol) = 18.26 - 0.103\ x.}$

As observed from Fig. (2-b) and deduced from the previous equation, which has a negative slope, the values of $\boldsymbol{V_M}$ decreased as the Cu-percentage was increased. This is a normal result, where the molar volume is inversely proportion to the density ($\rho_S^{exp} \alpha\ 1/V_M$). In addition, the molar volume of copper is less than that of germanium, (V_M of Cu = 7.11 (cm^3/mol), while V_M of Ge = 13.63 (cm^3/mol). Consequently, the $V_M -$ values decrease as the Cu-ratio was increased in the chalcogenide $Cu_xGe_{20-x}Se_{40}Te_{40}$ compositions.

The molar mass, M_M of the present bulk samples has also been calculated, then the estimated values were reported in Table 3, too. It was observed that the value of M_M decreases as the ratio of the presence of Cu was increased, as illustrated in Fig. (3-a). This decreasing is owing to the molar masses of Cu and Ge elements, where Ge was replaced by Cu. As reported in Table 1, M_M of the copper is smaller than that of germanium (M_M of the Cu = 63.55 gm/mol, while M_M of the Ge = 72.63 gm/mol). The plot of data evaluated of M_M versus the Cu-ratio, x, was linearly fitted to give the following empirical straight-line Eq.: $\boldsymbol{M_M\ (gm/mol) = 197.386 - 0.106\ x.}$

Moreover, The values of the excess volume, V_e of the present Cu-Ge-Se-Te bulk samples have also been calculated. Where, V_e is the difference between the theoretical and experimental molar volumes, i.e. $V_e = V^{th} - V_M$. Therefore, the theoretical molar volume, V^{th} must be firstly calculated to compute V_e. The Eq. (1) was used to determine V^{th}–values and then these values were tabulated in Table 3, too. Further, these $V^{th} -$ values depicted in Fig. (3-b) as a function of the Cu-percentage which it is best fitted linearly to get this experimental equation: $\boldsymbol{V^{th}(cm^3/mol) = 17.703 - 0.092\ x.}$

As obvious, the $V^{th} -$ values decrease as the Cu-ratio was increased, which is due to that the molar volume of Ge is larger than that of Cu, therefore, as Cu-content increases, V^{th}–value decreases. Thus, and knowing both V^{th} and V_M, It could now calculate the excess volume, V_e. Table 3 reports also these estimated values. Depending upon the values of each V^{th} and V_M, anyone can calculate the free volume percentage, *FVP*-values. The computed values of this parameter were also listed in Table 3. It is worth mentioning that the values of both V_e and *FVP* were independent upon the molar fraction value of the copper. The packing density, D_P is another parameter satisfies the bulk materials, it is the ratio of

Table 2
The experimentally measured EDS-ratios % and those of the selected and prepared values of the compositional element ratios of the a-Cu_x Ge_{20-x} Se_{40} Te_{40} samples.

a-Cu_x Ge_{20-x} Se_{40} Te_{40} Samples	Experimentally measured EDS-ratio at. %				Selected and prepared ratio at. %				Exp. errors ± %
	Cu	Ge	Se	Te	Cu	Ge	Se	Te	
Ge_{20} Se_{40} Te_{40}	0.000	20.198	39.660	40.142	00.00	20.00	40.00	40.00	0.99
Cu_5 Ge_{15} Se_{40} Te_{40}	4.874	14.471	40.988	39.667	05.00	15.00	40.00	40.00	0.96
$Cu_{10}Ge_{10}$ Se_{40} Te_{40}	10.148	10.423	39.878	39.551	10.00	10.00	40.00	40.00	0.98
Cu_{15} Ge_5 Se_{40} Te_{40}	14.933	5.126	39.979	39.962	15.00	05.00	40.00	40.00	0.99
Cu_{20} Se_{40} Te_{40}	19.305	0.000	40.148	40.547	20.00	00.00	40.00	40.00	0.98

Table 3
The determined experimental and theoretical density values and some other related physical parameters; as well as some atomic parameters of a-$Cu_xGe_{20-x}Se_{40}Te_{40}$ glassy samples.

The parameter	Chalcogenide $Cu_xGe_{20-x}Se_{40}Te_{40}$ glassy composition				
	$Ge_{20}Se_{40}Te_{40}$	$Cu_5Ge_5Se_{40}Te_{40}$	$Cu_{10}Ge_{10}Se_{40}Te_{40}$	$Cu_{15}Ge_5Se_{40}Te_{40}$	$Cu_{20}Se_{40}Te_{40}$
$\rho_S^{exp} \pm 1.3\%$ (gm/cm^3)	5.376	5.423	5.536	5.774	5.892
ρ_S^{th} (gm/cm^3)	5.489	5.606	5.728	5.855	5.988
M_m (gm/mol)	97.54	96.70	96.25	95.79	95.34
$V_m \pm 0.13$ (cm^3/mol)	18.144	17.831	17.386	16.590	16.181
V^{th} (cm^3/mol)	17.770	17.249	16.629	16.360	15.922
$V_e = V_m - V^{th}$(cm^3/mol)	0.374	0.582	0.757	0.230	0.259
FVP (%)	2.061	3.267	4.355	1.360	1.602
P_D10^{22} (Atom/cm^3)	3.318	3.418	3.553	3.619	3.724
Compactness, δ	−0.110	−0.051	−0.044	−0.018	−0.014
$AD_{Cu}10^{21}$ (Atom/cm^3)	0.000	2.485	5.050	7.863	10.648
$AD_{Ge}\times10^{21}$ (Atom/cm^3)	8.697	6.523	4.419	2.293	0.000
$AD_{Se}\times10^{22}$ (Atom/cm^3)	1.598	1.600	1.625	1.687	1.714
$AD_{Te}\times10^{22}$ (Atom/cm^3)	0.990	0.991	1.006	1.044	1.060
$AD_{Tot}\times10^{22}$(Atom/cm^3)	3.457	3.451	3.578	3.747	3.839
$IAS_{Se\text{-}Se}$ (Å)	3.970	3.968	3.948	3.899	3.878
$Rp_{\text{-}Se}$ (Å)	1.600	1.599	1.591	1.571	1.563
$FS_{Se}\times10^{15}$ (cm^{-2})	7.812	7.822	7.901	8.103	8.187
$IAS_{Te\text{-}Te}$ (Å)	4.657	4.655	4.632	4.575	4.552
$Rp_{\text{-}Te}$ (Å)	1.877	1.876	1.867	1.843	1.834
$FS_{Te}\times10^{15}$ (cm^{-2})	5.677	5.683	5.738	5.888	5.946

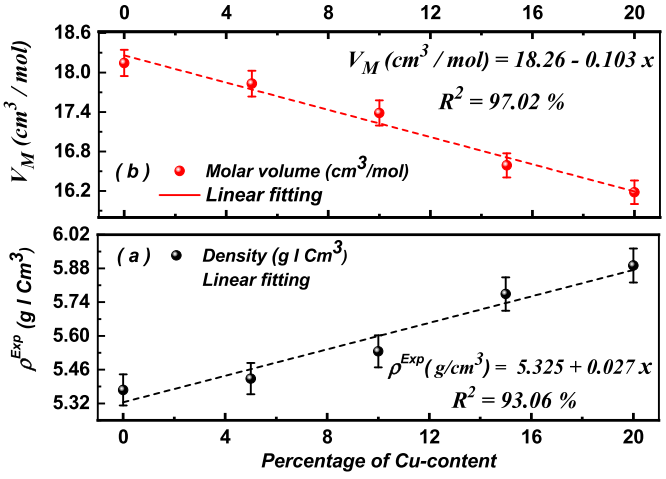

Fig. 2. Density and molar volume as functions of the percentage of Cu-concentration within the quaternary Cu_x Ge_{20-x} Se_{40} Te_{40} glasses.

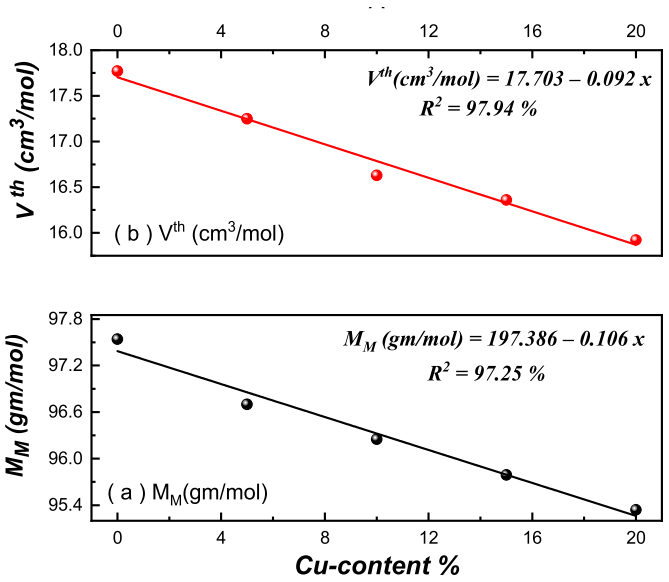

Fig. 3. Molar mass and theoretical molar volume as functions of the percentage of Cu-concentration in the quaternary Cu_x Ge_{20-x} Se_{40} Te_{40} glasses.

the used space to a selected one.

The values of this parameter D_p were calculated using Eq. (2) and tabulated in Table 3, too. Besides, the D_p-values were represented against the Cu-content percent in Fig. (4-a). The packing density, D_p of the present bulk samples were fitted to get this Eq.: $\boldsymbol{D_P\,(gm/cm^3) = 3.323 + 0.02\,x.}$ Here (x) is the Cu-percentage. On the other hand, the variation in the average atomic size of any substance, which is known as the compactness, **δ**, was calculated employing Eq. (3). This compactness originates due to the mutual chemical reactions between the atoms of that substance. The determined **δ**-values were recorded in Table 3 and represented graphically versus the Cu-content %, (x), as shown in Fig. (4-b). The figure was fitted to obtain this empirical linear form: $\boldsymbol{\delta = -0.092 + 0.005\,x.}$ Here, x is the Cu-molar fraction in the quaternary samples of Cu-Ge-Se-Te glasses.

4.3. Estimation of atomic densities, AD and their related parameters

Using the postulated form by Naster–Kingery, it could calculate the atomic densities, AD of the compositional elements of Cu-e-Se-Te samples. The computed AD values were evaluated and reported in Table 3, as well as illustrated in Fig. (5) as functions of the Cu-atomic ratio %. It can observe that the atomic intensity of Cu increased and that of Ge decreased as the ratio of Cu was increased, which is a normal result, where Cu replaced instead of Ge in the host Cu-e-Se-Te lattice. Thereby, the number of atoms of Cu per cubic cm must increase and those of Ge must decrease. On the other hand, the AD-values of both Sue and Tea are also increased when Cu-ratio increased, as shown also in Fig. (5). These graphs were fitted to get the following empirical linear Eqs.:

$$AD_{Cu} = (-0.126 + 0.533\ x) \times 10^{21}\ (atoms/cm^3)$$

$$AD_{Ge} = (8.711 - 0.432\ x) \times 10^{21}\ (atoms/cm^3)$$

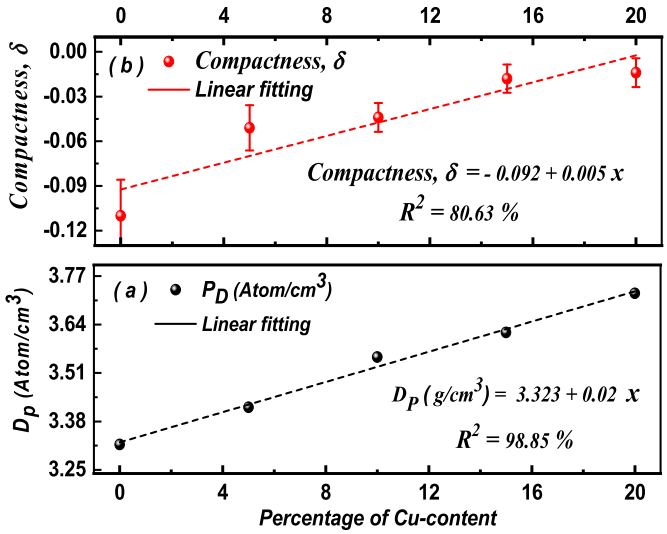

Fig. 4. Packing density and compactness as functions of the copper % within Cu-Ge-Se-Te glassy matrix.

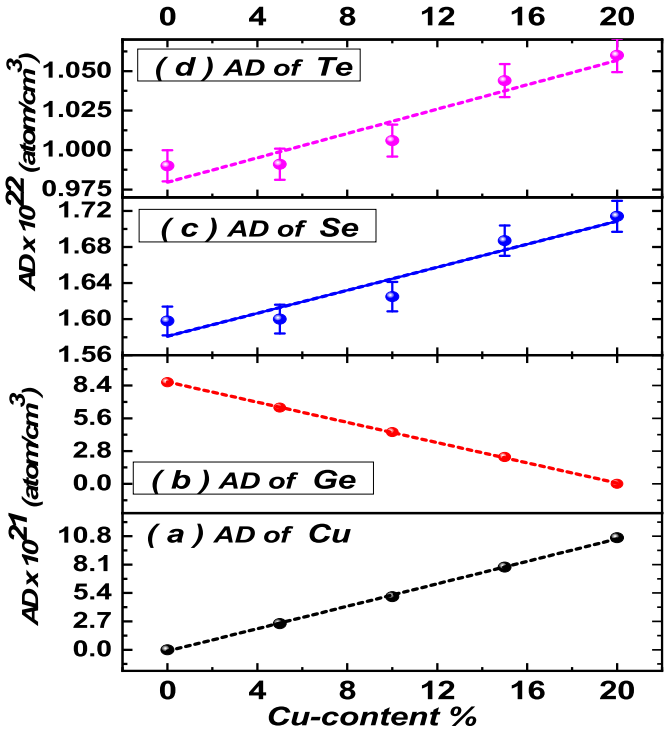

Fig. 5. Variation of the atomic densities of Cu, Ge, Se and Te elements of bulk Cu-Ge-Se-Te glassy samples as functions of the Cu-content %.

$AD_{Se} = (1.581 + 0.006\ x) \times 10^{22}$ (atoms/cm^3)

$AD_{Te} = (0.980 + 0.004\ x) \times 10^{2\ 2}$(atoms/cm^3)

Along with, the atomic density of the samples of the $Cu_xGe_{20-x}Se_{40}Te_{40}$ bulk compositions increased from 3.457 atoms/cm^3 to 3.839 atoms/cm^3 as the Cu-content % was increased from 0.0% to 20.0%, as reported in Table 3. Moreover, the interatomic separation between any two neighbor atoms, $IAS_{Atom-Atom}$ decreases between any two Se and between two Te atoms, too. For Se-element, IAS decreases from 3.970 Å to become 3.878 Å, and from 4.657 Å to 4.552 Å for Te, as depicted in Fig. (6-a). This is owing to that the interatomic separation distance is inversely proportional to the atomic density ($IAS \propto 1/AD$). Based on the estimated IAS-values, the polaron radius, Eq. (4), R_p of Se and Te can be estimated also. The polaron radius R_p-values could also be estimated and then recorded in Table 3. Moreover, it is also depicted as a function of Cu-ratio in the Fig. (6-b). For Se-element, R_p-values decrease from 1.600 Å to 1.563 Å, while for Te-element, decrease from 1.877 Å to 1.834 Å, as Cu-concentration increased from 0 to 20%. It is worth noting that the estimated polaron radii are greater than the atomic radii, whether it is the selenium atom or the tellurium atom. Where, the atomic radius of Se-atom, is $R_{Se} = 1.15$ Å, while for Tellurium atom, it is $R_{Te} = 1.40$ Å. These results are acceptable and in good consistency with the definition of the polaron radius. Where, the radius of the polaron must be larger than the atomic radius, R_{atom}. Moreover, the determined Rp-values are less than the interatomic separation distances, which are in good consistency with the theoretical hypothesis. Where, R_p must be larger than the atomic radius and less than the average interatomic spacing ($R_{atom} < R_p < IAS$) [42,65].

Furthermore, the values of the field strength, ***FS*** were also calculated for both Se- and Te- element. This parameter gives the atom-field strength that affects other atoms in its region and nearby. The obtained FS-values were tabulated also in Table 3 and presented as functions of the Cu-concentration percent in Fig. (6-c). It is observed that the FS-values increases from 7.812 × 10^{15} cm^{-2} to 8.187 × 10^{15} cm^{-2} for Se-atoms and from 5.677 × 10^{15} cm^{-2} to 5.946 × 10^{15} cm^{-2} for Te-atoms as the Cu-ratio increased from 0% to 20% in the Cu-Ge-Se-Te host lattice. The set of Fig. (6) have been linearly fitted to get the following empirical equations:

Interatomic distances: IAS_{Se-Se} (Å) = 3.983−0.005 x and IAS_{Te-Te} (Å) = 4.672−0.006 x

Polaron radius: R_{p-Se} (Å) = 1.605−0.002 x and R_{p-Te} (Å) = 1.883−0.002 x

Field Strength: FS_{Se} (cm^{-2}) = (7.759 + 0.021 x) × 10^{15} and FS_{Te} (cm^{-2}) = (5.638 + 0.015 x) × 10^{15}

4.4. Optical studies of Cu-Ge-Se-Te thin films

Chalcogenide thin-films are characterized by their excellent transmission and lower refractivity (which may tend to zero) in the near-infrared, NIR region, in addition, there is a shift of the absorption edge. This shift may occur towards lower energy values, i.e. towards the right along the curve that varied with the wavelength or towards higher energy values i.e. towards the left, depending upon many parameters, like the film thickness, the composition of the film sample itself and the doped material. In addition, the chalcogenide films characterized by their higher refractive index, which has values are arranged between 2 and 3.5 [34,66]. Moreover, the optical characteristics of these films are strongly influenced by the chemical bonds formed among the constituent materials of the film composition [34,66–68]. Therefore, in this work the authors will study and discuss the effect of composition upon some optical properties and the relation between the optical energy gap, Urbach energy and the cohesive energy of the quaternary $Cu_xGe_{20-x}Se_{40}Te_{40}$, CGST thin-film samples.

4.4.1. Transmittance and reflectance spectra

Figs. (7) illustrates the transmission spectra of chalcogenide $Cu_xGe_{20-x}Se_{40}Te_{40}$ thin films. This figure shows that the

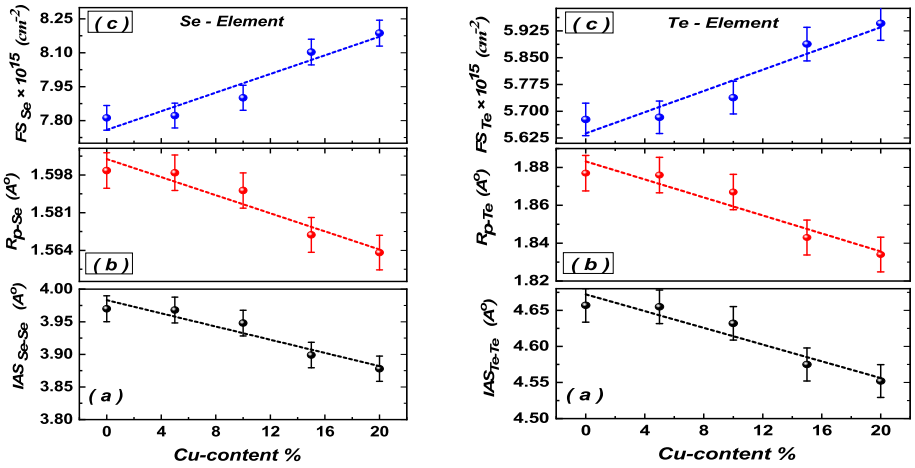

Fig. 6. Variations of (a) interatomic separations between any two neighbor atoms, IAS, (b) polaron radius, Rp and (c) the atomic field strength, FS versus the Cu-percentage for Se- and Te-elements within Cu-Ge-Se-Te glassy samples.

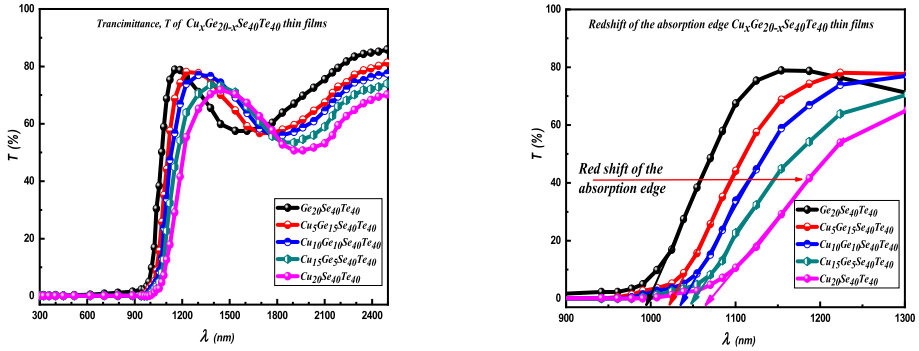

Fig. 7. (a) The dependence of T-spectra % upon λ, (b) the redshift of the absorption edge of Cu-Ge-Se-Te thin-films as increasing the Cu-ratio.

transmittance, T−values are very small, or it may be neglected, in the UV and visible regions, where the absorption of films is very high. But, at a wavelength equals ≈ 900−1100 nm, the value of the transmittance, T % increases suddenly, dramatically and very rapidly. Where, the transmittance value may reach to about 70−80% at a wavelength almost ranged from about 1100 nm to 1400 nm. Then, T−values decreases again and followed by an increasing again after ≈1800−2200 nm, to reach its maximum value almost after the wavelength of 2300. The value of T reaches about 83%, at a wavelength of ≈ 2350 nm, approximately. Furthermore, the transmission nature of CGST films decreases as the Cu-ratio increased, as shown in Figs. (7). This is due to the physical properties of the copper element, such as its opaque nature and high density in comparison with the germanium element.

In addition to the above mentioned, it can also find that there is a redshift of the absorption edge of film samples (i.e. towards higher wavelengths), where it is shifted from ≈ 995 nm to 1070 nm as the Cu-content was increased from 0.0% to 20.0%, as depicted in Fig. (7-b). The values of the wavelength of the absorption edge, $\lambda_{abs.-edge}$ of films is listed in Table 4. On the other hand, the variation of the reflectance spectra, R % versus the wavelength, λ of the films is illustrated in Fig. (8). It can see that the behavior of R-spectra is relatively opposite to that of T-spectra, where the film reflectivity increases as the Cu-percent is increased. Similar results have been reported for other semiconducting thin films [69,70]. Furthermore, behind the absorption edge of a-CGST films and at longer wavelengths, it can observe that $T + R \leq 1$, as exhibited in Figs. (7) and (8). Generally, the absorbance, A-value is given as $A = 1 - (T + R)$, which becomes very low or maybe neglected. This observation indicates that there is neither scattering nor absorption of light, i.e. these samples are non-dispersive samples. Thereby Cu-Ge-Se-Te can be used in the applications of optoelectronics devices, infrared imaging, and optical filters and detectors. These results affirm that the prepared a-CGST films have homogenous nature, smooth surface, and high-optical quality [22,34]. Moreover, the obtained T and R results are very consistent with some similar previous works [69−71].

4.4.2. Optical absorption studies

The study of absorption spectra is a pivotal issue as it plays a great role in controlling the optical properties of any material. It provides good information about both the type of electronic transition and the optical energy gap of the studied semiconductor materials, to be utilized in any potential application [34,41]. Along the spectra curves of the optical absorption of any non-crystalline, disordered or even the partially crystalline materials, there are three major special regions, they are: (1) the strongest absorption region at lower wavelengths, (2) the absorption edge region and (3)

Table 4
Obtained optical and physical parameters of a-$Cu_xGe_{20-x}Se_{40}Te_{40}$ samples.

The parameter	Quaternary $Cu_xGe_{20-x}Se_{40}Te_{40}$ thin-films				
	$Ge_{20}Se_{40}Te_{40}$	$Cu_5Ge_5Se_{40}Te_{40}$	$Cu_{10}Ge_{10}Se_{40}Te_{40}$	$Cu_{15}Ge_5Se_{40}Te_{40}$	$Cu_{20}Se_{40}Te_{40}$
$\lambda_{abs.\ edge}$ (nm)	995	1020	1037	1053	1070
E_g^{exp}, (eV)	1.208	1.155	1.105	1.065	1.045
E_g^{th} (eV)	0.966	0.933	0.899	0.866	0.833
E_U (eV)	0.186	0.191	0.199	0.210	0.219
$\sigma \times 10^{-2}$ (eV)	13.67	13.30	12.77	12.10	11.61
S_{e-p} $(eV)^{-1}$	4.877	5.012	5.221	5.510	5.742
$E_C(eV)$	1.099	1.549	1.999	2.591	3.184
N_C	2.400	2.250	2.100	1.950	1.800
$VE_{No.}$	5.600	5.750	5.900	6.050	6.200
LP	3.200	3.500	3.800	4.100	4.400
FM	0.000	0.125	0.250	0.375	0.500
N_{bb}	1.200	1.125	1.050	0.975	0.900
N_{bS}	1.800	1.500	1.200	0.900	0.600
$N_{Total\ Cont.}$	3.000	2.625	2.250	1.875	1.500
D_{CL}	1.000	0.625	0.250	−0.125	−0.500
$N_{C_{Eff}}$	4.200	4.050	3.100	2.950	2.800

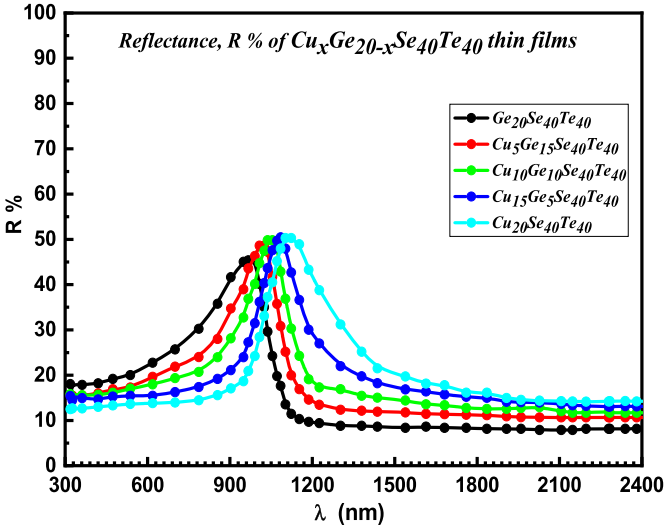

Fig. 8. The behavior of R-spectra versus λ for a-CGST films.

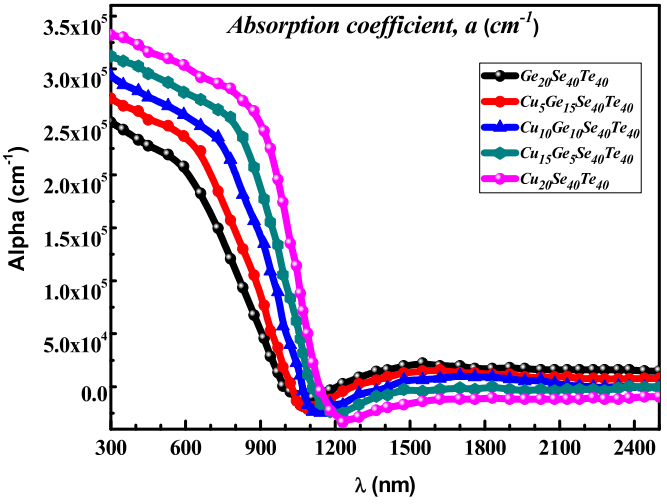

Fig. 9. The dependence of (α) on (λ) of a-Cu-Ge-Se-Te films.

the weak absorption region at longer wavelengths [5]. According to these three distinct regions, anyone can evaluate the optical band-gap energy, E_g from the first strongest absorption region, while the tail of the bandwidth or Urbach characteristic energy, E_U can be estimated from the second region. The third region of weak absorption is arisen owing to the formed defect localized states and the disorder of the semiconducting material [17,21]. Consequently, in the following sections, the authors have carefully studied this important curve for the amorphous CGST thin films, to determine both the optical gap energy, E_g and the Urbach energy, E_U and then studied the interrelationship between them.

4.4.2.1. Absorption coefficient and absorbance. The absorption coefficient, can be calculated using R and T-spectra from the following Eq. [41,71]:

$$\alpha(\lambda) = \frac{1}{t}.\ln\left(\frac{(1-R)^2}{2T} + \left(\frac{(1-R)^4}{4T^2} + R^2\right)^{1/2}\right) \quad (9)$$

where (t) is the thickness of the synthesized films. This equation has the advantage of considering the multiple internal reflections that may occur [72]. Hence, the absorption coefficient (α) has been computed and then depicted in Fig. (9) as a function of (λ). It can also be observed that at UV and Vis regions (i.e. at the high energy region and low wavelength, less than 1000 nm), the transmission values were very close to zero, while the absorption coefficient has high values. While in the near-infrared, NIR-region, which has lower energies and higher wavelengths (greater than 1200 nm), anyone can see that the transmission values are high values while the absorption coefficient values completely dwindle and may reach zero. It can also observe that, in the UV and Visible regions, the absorption coefficient values are increased as the Cu-ratio is increased, and their values are larger than 10^4 cm^{-1}.

Otherwise, the absorbance or the optical density, $D_{opt.}$ is a good quantitative term that indicates the light absorbed by a given substance. The importance of this parameter is since it reflects the quality and properties of the thin film, like its concentration, morphology, and suitability for use. The absorbance, D_{opt} can be computed from knowing both (α) and (t), where D_{opt} is given as $D_{opt} = \alpha t$ [34,67]. Thereby, $D_{opt.}$ of a-CGST thin films can be easily determined and then graphically illustrated. Fig. (10) shows the absorbance graph, $D_{opt.}$ of the a-CGST thin-film samples and its dependence on the incident wavelength, λ.

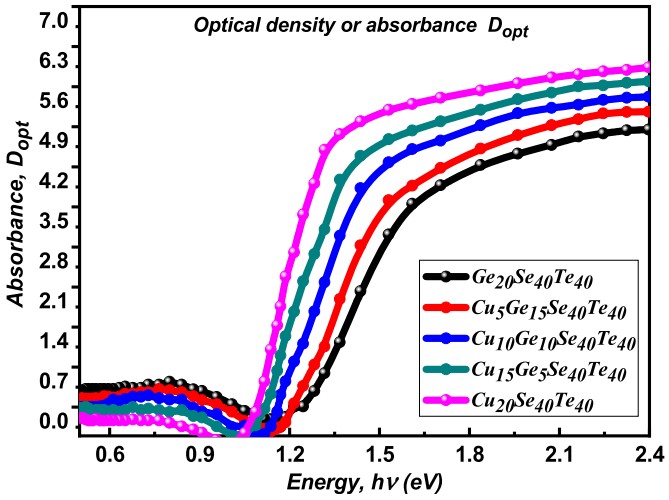

Fig. 10. The variation of (D_{opt}) with (λ) for a- CGST thin films.

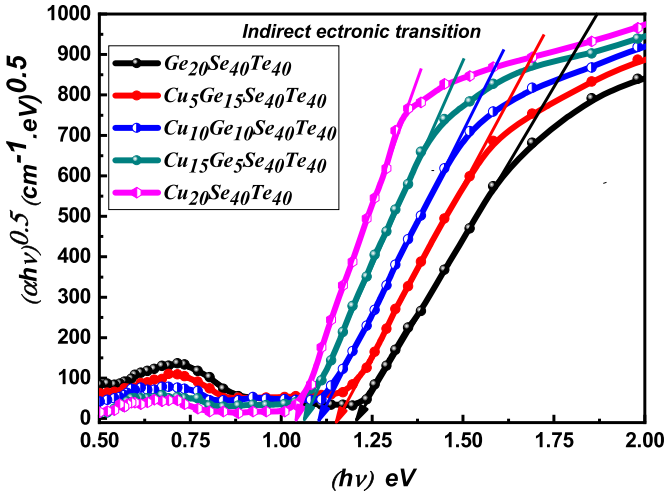

Fig. 11. Tauc's plot of the indirect allowed transition of amorphous CGST thin-film samples.

4.4.2.2. Tauc and Urbach energies. As proposed by Tauc and developed by Davis and Mott, the electronic transitions in semiconducting material are usually dependent on the material itself and the energy of the incident photons. Therefore, the strength of optical absorption is dependent upon the difference between the energy of the incident photon ($h\nu$) and the energy of the bandgap between the valence band and the conduction band (E_g) [73,74]. Tauc's graphical plots are often used to obtain the optical energy gap in semiconducting materials by knowing the absorption data and the wavelength of incident photons. This gap is frequently used to experimentally characterize the optical and electronic properties of semiconductors. Tauc's relation is given as follows [73–75]:

$$\alpha = \frac{A}{h\nu}(h\nu - E_g)^{1/n} \quad (10a)$$

or,

$$(\alpha h\nu)^n = A\,(h\nu - E_g) \quad (10b)$$

Noting that the exponent n is called the transition-mode power factor; it depends on whether the material is crystalline or non-crystalline. Moreover, its value is dependent on the electronic transition type, where it indicates the transition type and nature. According to Eq. (10-b), this exponent, n takes one or two values of the following values: 2 and 2/3, for the direct allowed and direct forbidden transitions, and for the indirect allowed and indirect forbidden transitions, n is 1/2 and 1/3, respectively. As obvious, the parameter (n) is dependent on the electronic transition; and A is some constant known as the band-tailing parameter [34,67,73,74].

Consequently, and according to Eq. (10-b) if anyone plot a graphical relation between $(\alpha h\nu)^n$ on the ordinate (y-axis) and $(h\nu)$on the abscissa (x-axis). Thus, the obtained graph contains a distinguished linear regime refers to the absorption onset of the material. Therefore, the extrapolation of this straight segment till it intersects the x-axis (hν-axis), then it can get the optical energy-gap value of the investigated material. For the present a-Cu-Ge-Se-Te thin films, and after several attempts to plot all probabilities for the value of n, it found that the value of n = 1/2 is the most suitable value for the present amorphous films, where it gave the longest straight segment to achieve what Davis and Mott imposed for non-crystalline solid semiconducting materials [74–76]. Consequently, the optical band-gap energy value of CuGeSeTe films could obtain and then tabulated in Table 4. Fig. (11) illustrates this

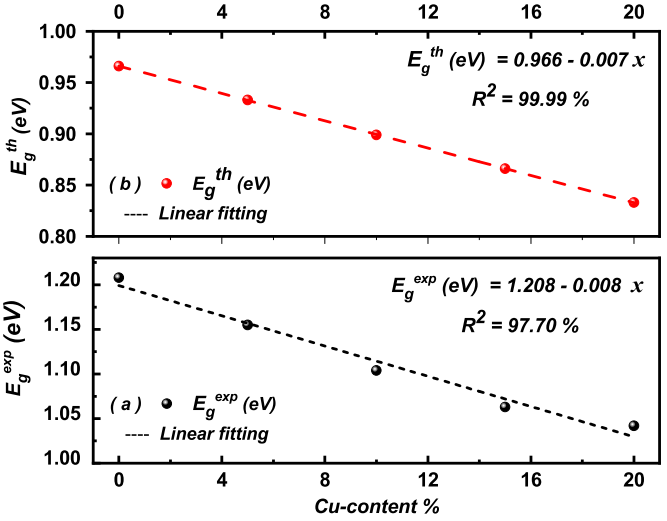

Fig. 12. Dependence of both (a) the experimental Tauc's band gap energy of amorphous CGST thin-film samples and (b)the theoretical bulk-glassy samples upon the Cu-concentration percent.

graphical indirect allowed transition of the deposited amorphous CGST thin-film samples to get Tauc energy values E_g. This figure exhibit that the value of E_g decreases from 1.208 eV to 1.045 eV as the Cu ratio increased from zero to 20% within the a-CGST film samples. These results are in complete harmony with the redshift of the absorption edge depicted in Fig. (7). Further, the obtained E_g^{exp} values of the a-CGST films are depicted as functions of (x) in Fig. (12-a). The graph is linearly fitted to get this empirical Eq.: $E_g^{exp}(eV) = 1.208 - 0.008\,x$.

Moreover, the band-gap energy was theoretically calculated for the bulk glassy samples using Shimakawa, Eq. (5) [51,52] and then tabulated in Table 4; then graphically illustrated as a function of the percentage of the Cu-content (x) percent within the amorphous CGST films in Fig. (12-b). The obtained figure is fitted to get a straight line has this Eq.: $E_g^{th}(eV) = 0.966 - 0.007\,x$. Here, (x) is the Cu-molar fraction ratio %. From Fig. (12), it is also worth to observe that the experimental and theoretical band-gap energy values have the same behavior, where both decreased as the Cu-content was

increased. But, the experimental energy values of the amorphous CGST thin-film samples are slightly larger than those of the theoretical bulk samples, which is a normal result, as assumed by Davis and Mott [74].

On the other hand, Urbach found that along the optical absorption coefficient curve and near the absorption edge of semiconducting non-crystalline or partially crystalline solid materials, there is an exponential part. This exponential part describes the band tail width of the material. This band tail is formed within the forbidden band gap and near the band edge of the valence and conduction bands of the non-crystalline materials. This tail represents the localized states within the band gap. These localized states lead to shrinking or diminish the width of the band gap. Urbach describes this assumption by an empirical equation interrelates between the absorption coefficient, (α) and the photon energy ($h\nu$). He formulated his assumption through the following Eq. [21,76]:

$$\alpha = \alpha_o \exp\left(h\nu / E_U\right) \tag{11a}$$

Taking the logarithm of the two sides of the last Eq. gives:

$$\text{Ln}\ \alpha = \text{Ln}\ \alpha_0 + \left(h\nu / E_U\right) \tag{11b}$$

where α_o is some constant, while the E_U is the band tail or the Urbach energy, it is independent of the temperature.

This energy describes the band tail width owing to localized states formed in the usual forbidden band gap associated with the disordered or non-crystalline materials. Thus, Urbach or band tail width energy (E_U) can be obtained from the reciprocal of the obtained straight-line slope of the graphical relationship between ln (α) represented on the Y-axis and the energy of the incident photon ($h\nu$) on the X-axis. While the intersection part of the Y-axis gives the value of the constant Ln (α_o). Fig. (13) illustrates this graphical plot, from which the value of the E_U and (α_o) can be determined. The obtained values of the E_U of the a-CGST thin films were computed from this figure and then reported in Table 4. It can observe that the band-tail energy, E_U increased from 0.186 eV–0.219 eV as Cu-percentage was increased from zero at. % to 20 at. %. Moreover, if a graphic relationship between the energy gap values (experimentally and theoretically) and the Urbach energy values was plotted and then linearly best fitted, as shown in Fig. (14), then anyone can get the following straight-line Eqs.:

$$E_g^{exp}\ (\text{eV}) = 2.070 - 4.748\ E_U$$

$$E_g^{th}\ (\text{eV}) = 1.674 - 3.456\ E_U$$

Furthermore, the obtained values of (E_U) were represented as a function of the elemental fractional percentage of the Cu-element (x) within the investigated CGSE films, as shown in Fig. (15-a) (Please, see Fig. 14). This figure was linearly fitted to obtain the following straight-line Eq:

$$E_U = 0.186 + 0.0017\ x$$

It should note that the E_U-values have an opposite behavior with the E_g-values, as shown in Figs. (15-a) and both (12-a) and (12-b), respectively; and from their empirical equations, too, where the two slopes or the values of x-coefficient are opposite to each other. These obtained results are a natural consequence as the decreasing of the band gap energy arises as a result of the formation of the localized states at the edge of the forbidden band. Thus, increasing the band tail width leads to decrease in the band-gap energy [34,67]. This result has been reported for the film samples of many chalcogenide non-crystalline materials [7,9,21,23].

Moreover, Urbach proposed also for the non-crystalline solid material another formula regarding the formed the localized states and band-tail width. He argued that the absorption coefficient, α can interrelate the optical band-gap energy by the following relation [76–79]:

$$\alpha = \beta \exp\left[\frac{\sigma(h\nu - E_o)}{KT}\right] \tag{12a}$$

where β is another constant differs from the constant α_o, (σ) is some constant called the steepness parameter. This parameter identifies the slope or the gradient of the straight segment of the absorption curve near the absorption edge [67–69]. While, E_o is the energy of the transition, in case of direct transition, it is equal to the band-gap energy, $E_o = E_g$, but for indirect transitions, it is equal to ($E_g + E_p$), where E_p is of the phonon energy associated with the indirect transition. Also, K is the Boltzmann' constant

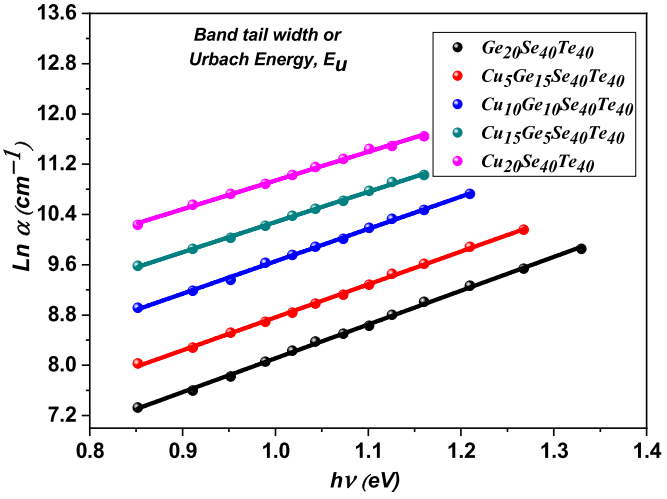

Fig. 13. Ln (α) Vs ($h\nu$) to get Urbach-band-tail-energy values of a-CGST film samples.

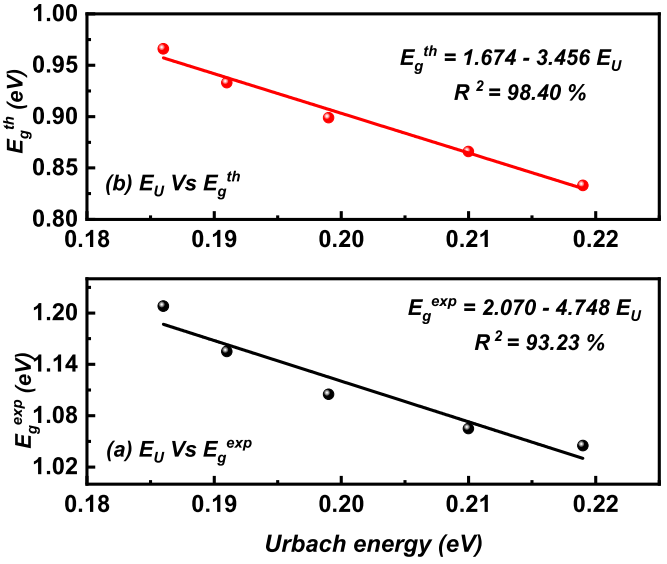

Fig. 14. The interrelationship between E_U and E_g- values of a-CGST thin films.

($K = 8.617 \times 10^{-5}$ eV/K) and T is the room temperature (295 K). Hence, taking the logarithm of the two sides of the last Eq., hence anyone can get the following form [67,77,78]:

$$\mathrm{Ln}^{\alpha} = \mathrm{Ln}^{\beta} + \left[\frac{\sigma(h\nu - E_o)}{KT}\right] \quad (12b)$$

Comparing between the two Eq. (12b) and (12-b) together, anyone can conclude that [41,67]:

$$\sigma = \frac{KT}{E_U} \quad (12c)$$

Consequently, the steepness parameter, σ could be estimated. The obtained values were scheduled in Table 4, and then they have graphically been exhibited in Fig. (15-b) as functions of the Cu-ratio (x), too. The graph is best linearly fitted, to obtain this empirical relation: $\sigma\,(eV) = 1.3674 - 0.0103\,x$. As obvious, the value of this steepness parameter decreased from 1.367 eV to 1.161 eV as the copper ratio increased. Moreover, there is a new optical parameter called the interaction strength between electron and phonon, $S_{e\text{-}p}$. This parameter describes the lattice expanding and increasing of the lattice constants. Increasing this parameter means increasing the lattice dimensions and vice versa. Taking into account that increasing the lattice dimensions leads to decreasing the band-gap energy. Hence, from the interrelationship between this optical parameter, σ and the interaction strength between electron and phonon during the electronic transition, $S_{e\text{-}p}$ which is given as follows [67,77]:

$$S_{e\text{-}p} = 2/3\sigma \quad (13)$$

Hence, anyone can calculate this crucial optical parameter, $S_{e\text{-}p}$. The estimated values of the phonon-electron strength have been also reported in Table 4, too. It can observe that the values of $S_{e\text{-}p}$ increased from 4.877 eV^{-1} to 5.742 eV^{-1} as the Cu-content % (x) was increased from 0.0% to 20%. This increasing behavior was also depicted and was linearly best fitted, as shown in Fig. (15-c) to get the following linear relation: $S_{e\text{-}p}\,(eV)^{-1} = 4.877 + 0.043\,x$. The increased interaction strength, Se-p values are in good correspondence with the decreased values of E_g. as they usually have an inverse proportion with each other. These results well affirm the correctness of the obtained values of E_g Ref. [67,77].

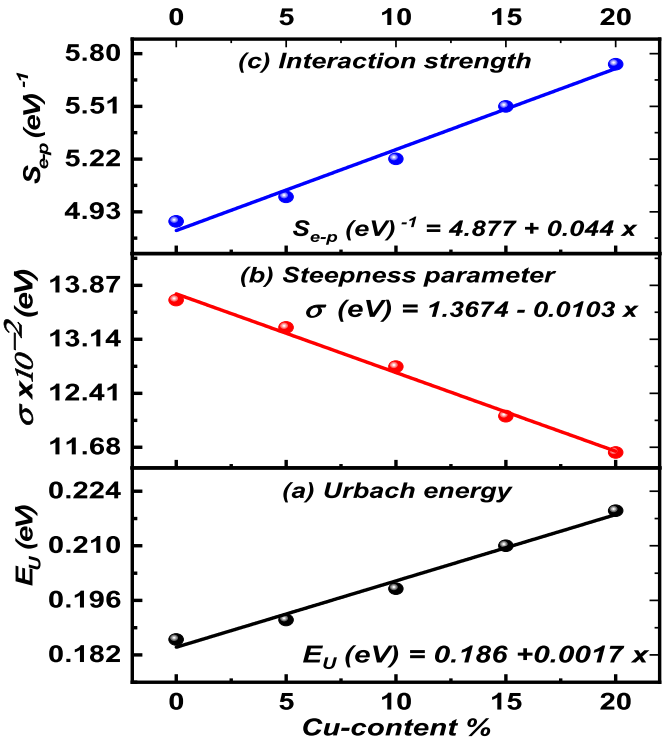

Fig. 15. Representation of the values of (a) Urbach energy, E_U, (b) the steepness parameter, σ, and (c) the interaction strength, $S_{e\text{-}p}$ between the electron and phonon as functions of the Cu-ratio of a-CGST thin films.

Therefore, and because of these good optical properties of a-CGST thin films, they can be used in many optoelectronic applications and devices, such as photovoltaics, solar cells, photonic circuits, photolithography, signal preparing, optical recorders, optical fibers and many others.

4.4.3. Chemical bond approach model, CBAM and determination of the cohesive energy, E_C

This model is a good quantitative method to investigate chalcogenide glassy semiconducting materials and their properties. Where, this method can give several worth insights about the probable chemical bonds that can form in the chalcogenide alloy or composition and hence the value of the cohesive energy, EC of that semiconducting material; along with the possibility that the average coordination number N_C of that network is principally interrelated to their vitrification properties, with the probability of finding special values of N_C resulting in the specific properties of that investigated network and then knowing and interpret them [54,80]. Hence, this CBAM is very beneficial in predicting the properties of the semiconducting material of different compositions. Consequently, the authors, in this section, will calculate the values of both EC and N_C and then correlate their values with the obtained optical band-gap energy values for the amorphous CuxGe20-xSe40Te40, CGST samples.

The cohesive energy values can be estimated using Eq. (6) after knowing the energy values of the heteronuclear bond that was computed by knowing the heteronuclear bond energies of the two elements and their electro-negativity values, χ_A and χ_B. Table 5 reports the evaluated hetero-nuclear and the known homonuclear bonds which may be formed among the constituent chemical elements of the quaternary $Cu_xGe_{20-x}Se_{40}Te_{40}$ samples. According to the CBAM, the possible amount of the formed heteronuclear and homonuclear bonds was calculated and reported also in Table 6. It can see that the increase of the Cu-content leads to an increase in the number of the strongest chemical bond, Cu—Te bond; this increment comes out at the expense of the less strong heteronuclear bond, Ge—Se bonds, which have lower energy and their number decreasing as Cu-content increased.

At the same time, the number of less strong heteronuclear bonds, which is the Se—Te bond, has little changes (a slight increase and then decreases again as before). On the other hand, the number of the weakest Te—Te homonuclear bond decreases and the strongest Se—Se homonuclear bond increased. All these changes lead to the increase of the cohesive energy of the quaternary a-$Cu_xGe_{20-x}Se_{40}Te_{40}$ samples as the Cu-element percentage increased. The calculated values of the cohesive energy, E_C of the present samples increase from 1.099eV to 3.184 eV as the Cu-content increased from 0.0% to 20.0%. All the obtained E_C-values of the present samples were listed in Table 4. So, it can conclude that the increment of the E_C-values is owing to the increase of the number the strongest bonds, Cu—Te, which have the largest energy value.

Furthermore, when someone wants to link between the optical band-gap energy values and those of cohesive energy values for each sample of the chalcogenide a-CGST network, he can recognize they have opposite behaviors to each other. While, with respect to

Table 5
The energy values of the heteronuclear and homonuclear bonds formed among the constituent elements of the quaternary samples of $Cu_xGe_{20-x}Se_{40}Te_{40}$ compositions [35,37,42,53,81].

The heteronuclear strongest bonds			The homonuclear defect bonds		
Formed bonds category	Energy of bonds		Formed bonds category	Energy of bonds	
	(kCal/mol)	(eV/atom)		(kCal/mol)	(eV/atom)
B(Cu–Te)	*278.7*	*12.092*	*B(Se–Se)*	*44.00*	*1.909*
B(Ge–Se)	*49.42*	*2.144*	*B(Te–Te)*	*33.00*	*1.432*
B(Se–Te)	*44.18*	*1.917*			
Bonds that are not formed Non formed bonds category					
B(Cu–Se)	*251.00*	*10.891*	*B(Cu–Cu)*	*176.52*	*7.659*
B(Cu–Ge)	*208.8*	*9.060*	*B(Ge–Ge)*	*37.00*	*1.605*
B(Ge–Te)	*35.47*	*1.539*			

Table 6
The chemical bonds formed within the a-$Cu_xGe_{20-x}Se_{40}Te_{40}$ samples and their number.

Chalcogenide samples	The chemical bonds formed within the sample of a-$Cu_xGe_{20-x}Se_{40}Te_{40}$ system						
	# Cu–Te bonds	# Ge–Se bonds	# Se–Te bonds	# Te–Te bonds	# Se–Se bonds	# all formed bonds	# formed defect bonds
$Ge_{20}Se_{40}Te_{40}$	00	20	20	20	00	60	20 (Te–Te)
$Cu_5Ge_{15}Se_{40}Te_{40}$	05	15	25	10	00	55	10 (Te–Te)
$Cu_{10}Ge_{10}Se_{40}Te_{40}$	10	10	30	00	00	50	00
$Cu_{15}Ge_5Se_{40}Te_{40}$	15	05	25	00	10	55	10 (Se–Se)
$Cu_{20}Se_{40}Te_{40}$	20	00	20	00	20	60	20 (Se–Se)

the Urbach energy (E_U), it can observe that both E_C and E_U increase as the Cu-content increases. The inversely proportional between the E_C and E_g has been represented graphically in Fig. (16-a), while Fig. (16-b) shows the direct proportion between the E_C and E_U. The figures were linearly fitted to get the following empirical Eqs.:

$$E_g^{exp}\ (eV) = 1.279 - 0.079\ E_C$$

$$E_U\ (eV) = 0.167 + 0.016\ E_C$$

Moreover, the increase of E_C presupposes a higher bonding strength, which results in decreasing the band-gap energy, E_g, owing to increment the defect bonds, which results in an increase in the Urbach energy [18,82]. Hurst and Davis (1974) [82,83] explicated these results via the suggestion that when the energy of the bond of the composition or alloy are not very different, the increase in the disorder that is related to the deviation from stoichiometry will lead to more pressing the mobility band-edges in the direction of their edges, hence diminishing the E_g-value. In general, these results are consistent with the results of many other similar amorphous ChG films [15,82–85].

4.4.4. The number of the average coordination and its related parameters

The number of the average coordination, $<N_C>$ is defined as the atom-averaged covalent coordination of the constituents of the chalcogenide material. This number, $<N_C>$ is a perfect tactic parameter for the covalent bonds to clarify the characters of atomic units of any composition [21,84]. Ioffe and Redel proposed that the bonding nature of the nearest neighbor zone is well-known in terms of this number [85,86]. To interpret the chalcogenide glassy structure, i.e. the continuous random network model, CRNM (the topological concepts) are utilized. The CRNM complies the principle of 8-N, where, N is the number of outer shell electrons. The values of this parameter, $<N_C>$ of ChG a-CGST samples have been estimated using Eq. (7) and then scheduled in Table 4, too. It can observe that the values of the average coordination number, $<N_C>$ decreased from 2.400 to 1.800. The decrease of the $<E_C>-$ values is owing to that the number of the valence electrons of Cu-element, (N = 1) is less than that of the Ge, (N = 4) and since the ratio of the copper increased at the expense of the ratio of germanium within the glassy CGST matrix [19].

Moreover, the value of the lone-pair electrons, LP of non-crystalline Cu-Ge-Se-Te samples can be also calculated by knowing the estimated values of both the number of valence electrons, $V_{No.}$ and the average coordinative number, $<E_C>$ [59–61,85]. The estimated values of $V_{No.}$ and LP have been calculated and then reported in Table 4. It can observe that, the number of valence electrons, $V_{No.}$ increased from 5.600 to 6.200, while the lone-pair electrons, LP increases from 3.200 to 4.400 as the Cu-content was increased. The scientist Z. Liang at 1991 had proposed in his approach that the chalcogenide material can keep its vitreous state if the LP-value of the composition is larger than 3. Hence, the alloy or the composition of the present studied Cu-Ge-

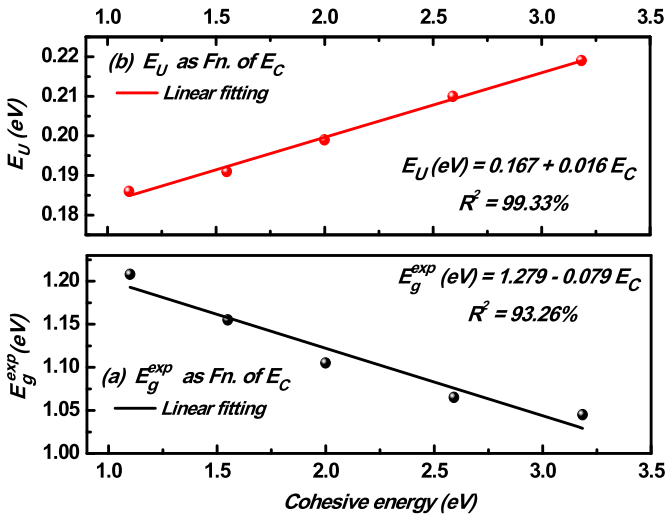

Fig. 16. The interrelationship between both the (a) band-gap energy and (b) Urbach energy, and the cohesive energy of a-CGST thin films.

Se-Te matrix, is a glassy one [59,86,87]. Consequently, and according to this approach, the present studied matrix is a good glassy matrix. This result can be attributed to the selenium atoms, which possess two couple of lone-pair electrons in its vitreous state [21], i.e. the investigated samples are rich in Se-content (40%).

It can observe that the existence of a large amount of Se-element in the glassy CGST matrix reduces the stress forces that give flexibility to a-CGST samples. This means that the formed chemical bonds become adaptive and tend towards the elastic region, which is confirmed by lower <NC> values. On the other hand, the floppy modes, FM of CGST glassy alloy, can be computed by knowing N_C-values. The determined FM-values were computed and listed in Table 4, too, they are increased from 0.00 to 0.50 as the Cu-ratio increased. This result confirms the obtained LP-values; hence these CGST glassy samples are good flexible alloys. Thus, Cu improved the mechanical properties, where it increases the sample flexibility and makes it has higher strength. Figs. (17-a), (17-b), (17-c) and (17-d) depicts both the decrement of <NC>-values and the increment of both the $V_{No.}$-, LP- and FM-values as the Cu-ratio increased, respectively. These figures have been best fitted to obtain the following linear experimental Eqns.:

For the average coordination number: $< N_C > = 2.40–0.03\ x$

For the total number of valence electrons: $V_{No.} = 5.60 + 0.03\ x$

For the number of the lone-pair electrons: $LP = 3.20 + 0.06\ x$

And, for the floppy mode's parameters: $FM = 0.00 + 0.025\ x$

These distinctive optical and physical properties make the Cu-Ge-Se-Te compositions are candidates for many applications, like the biomedical applications, reversible phase change, microsensing, switching and memory devices, electrochemical sensors, waveguides, light-emitting detectors, and infrared detectors.

4.4.5. *Mechanical constraints, N_{con}*

The total number of mechanical bond constraints, N_{con} of the present chalcogenide Cu-Ge-Se-Te glassy samples have been determined after determining the two constituent types of constraints; which the bond bending, N_{bb} and the bond stretching constraints, N_{bs} using Eq. (8-a) and (8-b) [45,48,62]. The computed values of both N_{bb}, N_{bs} and $N_{Total\ Cont.}$ have also listed in Table 4 and then graphically illustrated as functions of the copper percentage in Fig. (18-a), (18-b) and (18-c), respectively. These graphs have been constructed linearly to obtain the following experimental Eqs.:

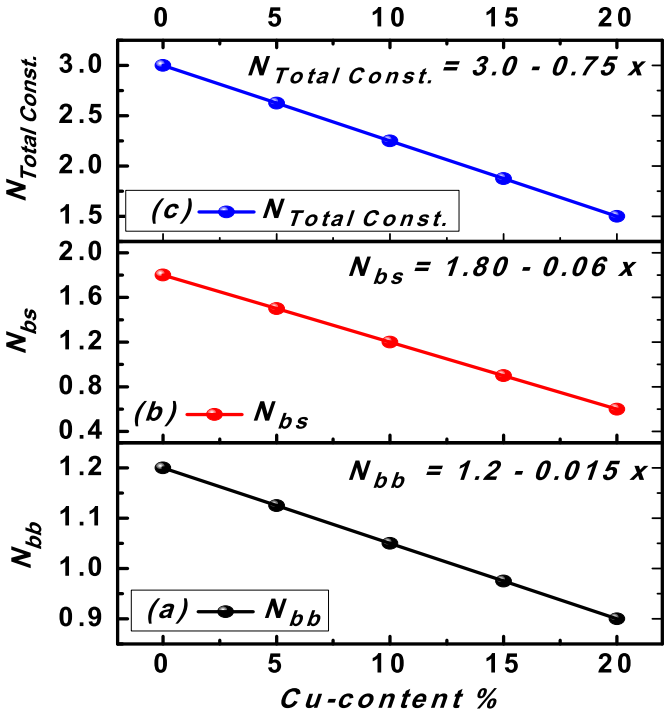

Fig. 18. Changing of both the number of (a) bond-bending constraints, N_{bb}, (b) bond-stretching constraints, N_{bs} and (c) the total mechanical-bond constraints, NTotal Cont as functions of the percentage of the copper ratio of CGST network.

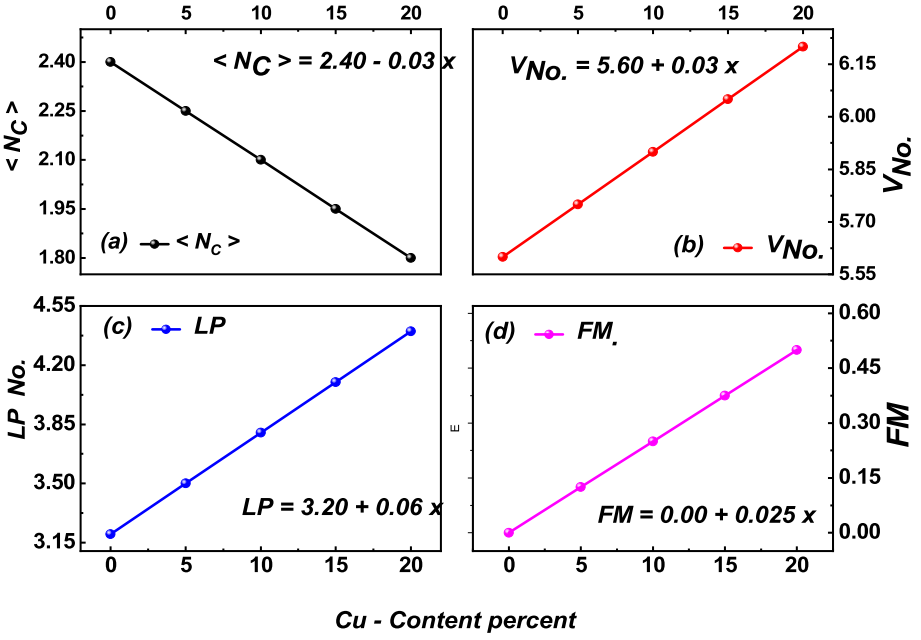

Fig. 17. Illustration of the variations of both (a) <NC>, (b)VNo., (c) LP and (d) FM versus the percentage of the Cu concentration % for a-CGST films.

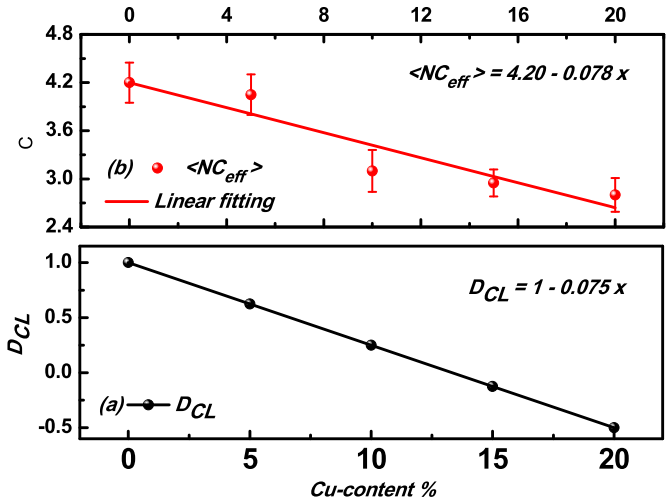

Fig. 19. Dependence of both (a) the cross-linking density values, DCL and (b) the effective coordination number, $N_{C_{Eff}}$ upon the Cu-content within the amorphous Cu-Ge-Se-Te thin films.

For the bond bending constraints, N_{bb}: Nbb = 1.20 − 0.015 x

For the bond stretching constraints, N_{bs}: Nbs = 1.80 − 0.060 x

While for the total number of mechanical bond constraints, $N_{Total\ Cont}$:

$N_{Total\ Const.}$ = 3.00 − 0.750 x

Moreover, the density of the cross-linking value, $\boldsymbol{D_{CL}}$ and the effective coordination number, $\boldsymbol{N_{C_{Eff}}}$ have also been determined using the computed values of the $N_{Total\ Cont}$, using Eqs. (19) and (20) [45,62]. Then, the calculated values have also reported in Table 4 and graphically plotted as functions of the Cu-ratio percent in Figs. (19-a) and (19-b), respectively. These graphs have been best linearly fitted to get the a set of these straight lines of the following experimental Eqs.:

For the cross − linking density values D_{CL}: DCL = 1 − 0.075 x

And for the effective coordination number, $\boldsymbol{N_{C_{Eff}}}$: <NCeff> = 4.20 − 0.078 x

5. Conclusions

This article was devoted to synthesizing Novel Non-Crystalline $Cu_xGe_{20-x}Se_{40}Te_{40}$, (x = 0, 5, 10, 15, 20 at. %), CGSE bulk gasses and thin-film samples and study their properties. Bulk and thin-film samples have been examined and investigated by X-ray diffraction, XRD and energy dispersive X-ray spectroscopy, EDS-technique. XRD exhibited that all studied CGSE samples have the non-crystalline nature. The authors have studied some decisive physical properties of the bulk CGSE glassy samples via measuring the mass-volume density. The authors have investigated and discussed the molar mass, molar volume, packing density, and the compactness, as well as the atomic density of elements, and others.

Many optical parameters and properties of $Cu_xGe_{20-x}Se_{40}Te_{40}$, thin films ($0.00 \leq x \leq 20.0\ at.\ \%$) have been discussed. Thin-film samples showed higher transmittance and lower reflectivity in the NIR region, which means that there is neither scattering nor absorption of the incident light. The authors have also studied the absorption coefficient, optical density, electronic transition, band-tail width via Tauc's plots and Urbach rule. The optical energy gap, E_g and Urbach energy, E_U have been determined for CGST films. These two energy parameters have opposite behavior, where E_g decreased from 1.208 eV to 1.045 eV, while E_U values increased from 0.186 eV to 0.219 eV as Cu-ratio increased from 0.00% to 20.0%. The authors have also estimated the values of the steepness parameter and electron phonon interaction forces. The Cu-doping increased both the optical and electrical conductivities. Further, it also decreases both the optical band gap and the steepness constant, while increases both the absorption coefficient value, the band tail width, and the strength of the electron-phonon interaction. The studied optical properties confirm the high quality and good homogeneity of film samples.

Furthermore, the chemical bond approach model was also employed to study the cohesive energy, E_C of the studied CGST samples. It was found that the value of the cohesive energy increased from 1.099 eV to 3.184 eV, while the number of the average coordination, $<N_C>$ decreased from 2.400 to 1.800, as Cu increased from zero to 20.0%. Based on the assigned values of $<N_C>$, many crucial parameters were assigned for the CGST samples. The studied physical and structural properties affirmed that the present CGST samples are good stable glassy materials, where the value of the lone-pair electrons increases from 3.200 to 4.400 and these samples can keep their vitreous state where the LP-values of samples are larger than 3.00. The present CGST bulk glasses are good flexible alloys, too, where the FM-values increased from 0.00 to 0.50. Increasing the Cu-ratio increased the chemical stability of the composition. In addition, Cu improved the mechanical properties, where it increases the sample flexibility and makes it has higher strength.

Funding

This research was not funded by any authority, entity or individual other than the authors themselves. The authors have born all the costs of the work.

Credit authorship contribution statement

Ahmed Saeed Hassanien: Conceptualization, Idea, Methodology, Formal analysis, Writing, original draft, Investigation, Supervision, Project administration, Resources, Visualization; I. M. El Radaf: Formal analysis, Writing, Review & editing, Project administration, Resources, Visualization; Alaa A. Akl: Formal analysis, Data curation, Project administration, Resources, Validation.

Declaration of competing interest

The authors declare that they have no known competing financial interests or personal relationships that could have appeared to influence the work reported in this paper.

References

[1] M. Isik, H.H. Gullu, E. Coskun, N.M. Gasanly, Optical band gap and dispersion of optical constants of Cu-Ga-S thin films, Optik 186 (2019) 147–154.
[2] D.K. Sharma, S. Hirata, L. Bujak, V. Buji, T. Kameyama, M. Kishi, T. Torimoto, M. Vacha, Single-particle spectroscopy of I-III-VI semiconductor nanocrystals: spectral diffusion and suppression of blinking by two-color excitation, Nanoscale 8 (2016) 13687–13694.

[3] C. Mahendran, N. Suriyanarayanan, Synthesis and characterization of sprayed Zn-doped polycrystalline CuInS2 thin films, Optik 124 (2013) 5089–5094.
[4] A.S. Hassanien, A.A. Akl, Electrical transport properties and Mott's parameters of chalcogenide cadmium sulphoselenide bulk glasses, J. Non-Cryst. Solids 432 (2016) 471–479.
[5] A.S. Hassanien, A.A. Akl, Influence of thermal and compositional variations on conduction mechanisms and localized state density of amorphous $Cd_{50}S_{50-x}Se_x$ thin films, J. Non-Cryst. Solids 487 (2018) 28–36.
[6] S.Q. Li, X.S. Tang, Z.G. Zang, Y. Yao, Z.Q. Yao, H.Z. Zhong, B.K. Chen, I-III-VI chalcogenide semiconductor nanocrystals: synthesis, properties, and applications, Chin. J. Catal. 39 (2018) 590–605.
[7] M.S. AlKhalifah, I.M. El Radaf, M.S. El-Bana, New window layer of $Cu_2CdSn_3S_8$ for thin film solar cells, J. Alloys Compd. 813 (2020) 152169.
[8] A. Kumar Singh, A Short over view on advantage of chalcogenides glassy alloys, J. Non-Oxide Glasses 3 (1) (2012) 1–4.
[9] H.H. Hegazy, A. Dahshan, K.A. Aly, Influence of Cu content on physical characterization and optical properties of new amorphous Ge-Se-Sb-Cu thin films, Mater. Res. Express 6 (2) (2019), 025204.
[10] S.R. Alharbi, K.A. Aly, Electrical and thermoelectric properties of ternary Cu-Ge-Te films, J. Alloys Compd. 797 (2019) 710–716.
[11] Garima, Ishu Sharma, S.K. Tripathi, The effect of substitution of Sb with Zn on the optical and physical properties of $Se_{90}Sb_{10-x}Zn_x$ (x = 0, 2, 4, 6, 10 at. %) thin films, Optik 207 (2020) 164460.
[12] A.S. Hassanien, R. neffati, K.A. Aly, Impact of Cd-addition upon optical properties and dispersion parameters of thermally evaporated $Cd_xZn_{1-x}Se$ films: discussions on bandgap engineering, conduction and valence band positions, Optik 212 (2020) 164681.
[13] S.A. Fayek, M.R. Balboul, K.H. Marzouk, Optical, electrical and thermal studies on $(As_2Se_3)_{3-x}$ $(As_2Te_3)_x$ glasses, Thin Solid Films 515 (18) (2007) 7281–7285.
[14] P. Kumar, S.K. Tripathi, I. Sharma, Effect of Bi addition on the physical and optical properties of $Ge_{20}Te_{74-x}Sb_6Bi_x$ (x = 2, 4, 6, 8, 10) thin films deposited via thermal evaporation, J. Alloys Compd. 755 (2018) 108–113.
[15] I. Sharma, S. R. Madara, P. Sharma, Study of Tauc gap, optical density and penetration depth of vacuum evaporated Pb_{15}-$Se_{85-x}Ge_x$ (x = 0, 3, 6 at. %) thin films supported by CBA and physical parameters, Mater. Today: Proceedings, https://doi.org/10.1016/j.matpr.2019.10.023
[16] H. El-Zahed, Optical absorption study of amorphous $Cu_xGe_{20-x}Te_{80}$ films as a function of composition, Physica B 307 (2001) 95–104.
[17] P.K. Singh, S.K. Tripathi, D.K. Dwivedi, Effect of thermal annealing on structural and optical properties of in doped Ge-Se-Te chalcogenide thin films, Mater. Sci. Pol. 37 (4) (2019) 554–562.
[18] S.A. Fayek, M.M. El-Ocker, A.S. Hassanien, Optical and electrical properties of $Ge_{10+x}Se_{40}Te_{50-x}$ thin film, Mater. Chem. Phys. 70 (2001) 231–235.
[19] M.M. El-Ocker, S.A. Fayek, F. Metawe, A.S. Hassanien, Thermal behaviour and non-isothermal kinematics of $Ge_{10}Se_{40}Te_{50}$ amorphous system, Indian J. Phys. 16 (72) (1998) 31–42.
[20] S.A. Fayek, M.M. El-Ocker, A.S. Hassanien, Optical and electrical properties of $Ge_{10+x}Se_{40}Te_{50-x}$ thin film, J. Mater. Res. 16 (6) (2001) 1549–1553.
[21] A.S. Hassanien, Ishu Sharma, Band-gap engineering, conduction and valence band positions of thermally evaporated amorphous $Ge_{15-x}Sb_xSe_{50}Te_{35}$ thin films: influences of Sb upon some optical characterizations and physical parameters, J. Alloys Compd. 798 (2019) 750–763.
[22] A.S. Hassanien, I. Sharma, Optical properties of quaternary a-$Ge_{15-x}Sb_xSe_{50}Te_{35}$ thermally evaporated thin-films: refractive index dispersion and single oscillator parameters, Optik 200 (2020) 613415.
[23] A.S. Hassanien, I. Sharma, A.A. Akl, Physical properties of $Ge_{15-x}Sb_xSe_{50}Te_{35}$ glassy bulk samples: refractive index and its association with electronic polarizability of thermally evaporated a-Ge-Sb-Se-Te thin-films, J. Non-Cryst. Solids 531 (2020) 119853.
[24] I.M. El Radaf, H.Y.S. Al-Zahrani, A.S. Hassanien, Novel Synthesis, structural, linear and nonlinear optical properties of p-type kesterite nanosized Cu_2MnGeS_4 thin films, J. Mater. Sci. Mater. Electron. (2020), https://doi.org/10.1007/s10854-020-03369-9.
[25] A.S. Hassanien, I.M. El Radaf, Optical characterizations of quaternary Cu_2MnSnS_4 thin films: novel synthesis process of film samples by spray pyrolysis technique, Physica B 585 (2020) 412110.
[26] A.A. Akl, I.M. El Radaf, A.S. Hassanien, Intensive comparative study using X-Ray diffraction for investigating microstructural parameters and crystal defects of the novel nanostructural ZnGa2S4 thin films, Superlattice. Microst. (2020), https://doi.org/10.1016/j.spmi.2020.106544.
[27] I.M. El Radaf, Structural, optoelectrical, linear, and nonlinear optical characterizations of the $Cu_2ZnGeSe_4$ thin films, J. Mater. Sci. Mater. Electron. (2020), https://doi.org/10.1007/s10854-020-02871-4.
[28] Z.U. Borisova, Glassy Semiconductor, Plenum, New York, 1985, p. 463.
[29] A.Y. Abdel-Latief, Kinetic study of non-isothermal crystallization in $Cu_xGe_{20-x}Te_{80}$ chalcogenide glasses, Physica B 311 (2002) 348–355.
[30] H.H. Hegazy, Semiconducting chalcogenide Ge-Se-Sb-Cu as new prospective thermoelectric materials, Res. Phys. 14 (2019) 102492.
[31] S.R. Alharbi, K.A. Aly, Electrical and thermoelectric properties of ternary Cu-Ge-Te films, J. Alloys Compd. 797 (2019) 710–716.
[32] Mathieu Hubert, Chalcogenide Glasses for Infrared Applications: New Synthesis Routes and Rare Earth Doping, Ph.D. Dissertation Submitted to University of Arizona, Department of Materials Science and Engineering, 2012.
[33] A. Dahshan, New amorphous As–Se–Sb–Cu thin films: theoretical characterization and evaluation of optical constants, Appl. Phys. A 123 (2017) 210.
[34] A.S. Hassanien, A.A. Akl, Influence of composition on optical and dispersion parameters of thermally evaporated non-crystalline $Cd_{50}S_{50-x}Se_x$ thin films, J. Alloys Compd. 648 (2015) 280–290.
[35] R. David Lide (Ed.), CRC Handbook of Chemistry and Physics, 88th edition, Taylor & Francis Group, Boca Raton, Florida, 2008.
[36] L. Pauling, The Nature of the Chemical Bonds, third ed., Cornell University Press, Ithaca, NY, 1960.
[37] Samuel Ruben, Handbook of the Elements, January 8, Open Court Publishing Company, La Salle, 1999. Illinois 61301.
[38] N. Sharma, S. Sharda, V. Sharma, P. Sharma, Far-infrared investigation of ternary Ge–Se–Sb and quaternary Ge–Se–Sb–Te chalcogenide glasses, J. Non-Cryst. Solids 375 (2013) 114–118.
[39] A.A. Akl, A.S. Hassanien, Microstructure and crystal imperfections of nanosized CdS_xSe_{1-x} thermally evaporated thin films, Superlattice. Microst. 85 (2015) 67–81.
[40] A.S. Hassanien, A.A. Akl, X-ray studies: CO_2 pulsed laser annealing effects on the crystallographic properties, microstructures and crystal defects of vacuum-deposited nanocrystalline ZnSe thin films, CrystEngComm 20 (2018) 7120–7129.
[41] A.S. Hassanien, A.A. Akl, Optical characteristics of iron oxide thin films prepared by spray pyrolysis technique at different substrate temperatures 124 (2018) 752.
[42] A.S. Hassanien, A.A. Akl, Estimation of some physical characteristics of chalcogenide bulk $Cd_{50}S_{50-x}Se_x$ glassy systems, J. Non-Cryst. Solids 428 (2015) 112–120.
[43] I. Sharma, A.Z. Khan, An assessment of topology and compositional dependent physical parameters of Ge-Se-Te-Bi lone pair semiconductors, J. Optoelectron. Adv. Mater. 19 (2017) 11–12, 778-787.
[44] A. Dahshan, K.A. Aly, Characterization of new quaternary Ge20Se60Sb20−xAgx (0 ≤ x ≤ 20 at.%) glasses, J. Non-Cryst. Solids 408 (2015) 62–65.
[45] I. Sharma, S. Sunder, Analysis of glass forming ability using percolation concept and tunability of physical parameters of a-$Ge_{12}Se_{76-x}As_{12}Bi_x$ glassy semiconductors, Mater. Sci. Pol. 36 (2) (2018) 242–254.
[46] S. Sharda, N. Sharma, P. Sharma, V. Sharma, Finger prints of chemical bonds in Sb–Se–Ge and Sb–Se–Ge–In glasses: a Far-IR study, J. Non-Cryst. Solids 362 (2013) 136–139.
[47] V. Pamukchieva, A. Szekeres, M. Todorova, E. Svab, Z.S. Revay, L. Szentmiklosi, Evaluation of basic physical parameters of quaternary Ge–Sb-(S,Te) chalcogenide glasses, J. Non-Cryst. Solids 355 (2009) 2485–2490.
[48] M. Vlcek, M. Frumar, Model of photoinduced changes of optical properties in amorphous layers and glasses of Ge-Sb-S, Ge-S, As-S and As-Se systems, J. Non-Cryst. Solids 97 (1987) 1223–1226.
[49] H.H. Naster, W.D. Kingery, in: Proceedings of the Seventh International Conference on Glass, Gordon and Breach, Brussels, 1965, p. 106. New York.
[50] M. Farouk, A. Samir, M. El Okr, Effect of alkaline earth modifier on the optical and structural properties of Cu2+ doped phosphate glasses as a bandpass filter, Phys. B Condens. Matter 530 (2018) 43–48.
[51] C. Xing, Y. Zhang, W. Yan, L. Guo, Band structure-controlled solid solution of $Cd_{1-x}Zn_xS$ photocatalyst for hydrogen production by water splitting, Int. J. Hydrogen Energy 31 (2006) 2018–2024.
[52] M. Askari, N. Soltani, E. Saion, W.M. Mat Yunus, H.M. Erfani, M. Dorostkar, Structural and optical properties of PVP-capped nanocrystalline $Zn_xCd_{1-x}S$ solid solutions, Superlattice. Microst. 81 (2015) 193–201.
[53] A.S. Hassanien, Studies on dielectric properties, opto-electrical parameters and electronic polarizability of thermally evaporated amorphous $Cd_{50}S_{50-x}Se_x$ thin films, J. Alloys Compd. 671 (2016) 566–578.
[54] J. Bicerano, S.R. Ovshinsky, Chemical bond approach to the structures of chalcogenide glasses with reversible switching properties, J. Non-Cryst. Solids 74 (1985) 75–84.
[55] P.K. Singh, S.K. Sharma, S.K. Tripathi, D.K. Dwivedi, Study of dielectric relaxation and thermally activated a.c. conduction in multicomponent $Ge_{10-x}Se_{60}Te_{30}In_x$ (0 ≤ x ≤ 6) chalcogenide glasses using CBH model, Respir. Physiol. 12 (2019) 223–236.
[56] A. Kumar, V. Singh, H. Singh, P. Sharma, N. Goyal, Electronic transport properties of $(Se_{80}Te_{20})_{100-x}Zn_x$ (2 ≤ x ≤ 6) chalcogenide alloys, Physica B 555 (2019) 41–46.
[57] B. Chen, G. Chen, W. Wang, H. Cai, L. Yao, S. Chen, Z. Huang, Magnetron sputtering deposition of GeSe thin films for solar cells, Sol. Energy 176 (2018) 98–103.
[58] A. Hosseinkhani, M. Tavoosi, A. Ghasemi, The optical, structural and thermal optimizations of Ge-As-Se-S-Te glasses, Infrared Phys. Technol. 85 (2017) 421–430.
[59] Z. Liang, Chemical bond approach to the chalcogenide glass forming tendency, J. Non-Cryst. Solids 127 (1991) 298–305.
[60] H. Ticha, L. Tichy, N. Rysava, Trisha, A study of nonlinear optical properties in Bi2O3–WO3–TeO2 glasses, J. Non-Cryst. Solids 354 (2008) 3468–3472.
[61] P. Kumar, S.K. Tripathi, I. Sharma, Effect of Bi addition on the physical and optical properties of $Ge_{20}Te_{74-x}Sb_6Bi_x$ (x = 2, 4, 6, 8, 10) thin films deposited via thermal evaporation, J. Alloys Compd. 755 (2018) 108–113.
[62] M.F. Thorpe, Continuous deformations in random networks, J. Non-Cryst. Solids 57 (1983) 355–370.
[63] A.S. Hassanien, A.A. Akl, Optical characterizations and refractive index dispersion parameters of annealed TiO_2 thin films synthesized by RF-sputtering technique at different flow rates of the reactive oxygen gas,

Physica B 576 (2020) 411718.
[64] A.S. Hassanien, A.A. Akl, A.H. Saaedi, Synthesis, crystallography, microstructure, crystal defects, and morphology of $Bi_xZn_{1-x}O$ nanoparticles prepared by sol–gel technique, CrystEngComm 20 (2018) 1716–1730.
[65] S.S. Fouad, M.S. El-Bana, P. Sharma, V. Sharma, Analysis of chemical ordering and fragility for Ge–Se–In glasses, Appl. Phys. A 120 (2015) 137.
[66] E.R. Shaaban, Calculation of the optical constants of amorphous semiconducting $As_{40}s_{60}$, $As_{40}s_{35}se_{25}$ and $As_{40}se_{60}$ thin films from transmittance and reflectance measurements, J. Appl. Sci. 6 (2006) 340–346.
[67] A.S. Hassanien, A.A. Akl, Effect of Se addition on optical and electrical properties of chalcogenide CdSSe thin films, Superlattice. Microst. 89 (2016) 153–169.
[68] A.S. Hassanien, K.A. Aly, A.A. Akl, Study of optical properties of thermally evaporated ZnSe thin films annealed at different pulsed laser powers, J. Alloys Compd. 685 (2016) 733–742.
[69] I.M. El Radaf, R.M. Abdelhameed, Surprising performance of graphene oxide/tin dioxide composite thin films, J. Alloys Compd. 765 (2018) 1174–1183.
[70] A.A. Yadav, E.U. Masumdar, Optical and electrical transport properties of spray deposited $CdS_{1-x}Se$ thin films, J. Alloys Compd. 505 (2010) 787.
[71] M.M. ELnahass, E. Eleshb, A. Gamal, Structural and optical properties of nanoparticles of tetraphenyl Porphin cobalt (II) annealed thin films, Optik 202 (2020) 163597.
[72] M. Giulio, G. Micocci, R. Rella, P. Siciliano, A. Tepore, Optical absorption of tellurium suboxide thin films, Phys. Status Solidi 136 (1993) 101.
[73] J. Tauc, Optical properties and electronic structure of amorphous Ge and Si, Mater. Res. Bull. 3 (1968) 37–46.
[74] E.A. Davis, N.F. Mott, Conduction in non-crystalline systems V. Conductivity, optical absorption and photoconductivity in amorphous semiconductors, Philos. Mag. A 22 (179) (1970) 903–922.
[75] J. Tauc, in: Amorphous and Liquid Semiconductors, Plenum Press, London and New York, 1974.
[76] F. Urbach, The long-wavelength edge of photographic sensitivity and of the electronic absorption of solids, Phys. Rev. 92 (1953) 1324.
[77] G.V. Makhnovets, G.L. Myronchuk, L.V. Piskach, B.V. Vidrynskyi, A.H. Kevshyn, Study of optical absorption in $TlGaSe_2:Zn^{2+}$ single crystals, Ukr. J. Phys. Opt. 19 (1) (2018) 49–59.
[78] I. Studenyak, M. Kranjec, M. Kurik, Urbach rule in solid state Physics, Int. J. Optic. Appl. 4 (3) (2014) 76–83.
[79] M. Karimi, M. Rabiee, F. Moztarzadeh, M. Tahriri, M. Bodaghi, Controlled synthesis, characterization and optical properties of CdS nanocrystalline thin films via chemical bath deposition (CBD) route, Curr. Appl. Phys. 9 (2009) 1263.
[80] J. Bicerano, S.R. Ovshinsky, Chemical bond approach to glass structure, J. Non-Cryst. Solids 75 (1985) 169–176.
[81] A. Kaistha, V.S. Rangra, P. Sharma, Assessment of physical parameters for quaternary antimony substituted Ge-Se-Te alloys, Glass Phys. Chem. 41 (2) (2015) 175–179.
[82] K.A. Aly, H.H. Amer, A. Dahshan, Optical constants of thermally evaporated Se–Sb–Te films using only their transmission spectra, Mater. Chem. Phys. 113 (2009) 690–695.
[83] C. Hurst, E.A. Davis, in: J. Stuke, W. Brenig (Eds.), Amorphous and Liquid Semiconductors, Taylor and Francis, London, 1974.
[84] MSc Thesis A.A. Abdel-Wahab, Study of the Physical Properties of Some Semiconductor Materials, Submitted for Physics Department, Faculty of Science, Helwan University, 2012.
[85] Sharma I., Hassanien A.S., Effect of Ge-addition on physical and optical properties of chalcogenide Pb10Se90-xGex bulk glasses and thin film, J. Non-Crystalline Solids 548 (2020) 120326, https://doi.org/10.1016/j.jnoncrysol.2020.120326.
[86] A.F. Ioffe, A.R. Redel, Progress in Semiconductors, vol. 4, John Wiley & Sons, Inc., New York, 1960, p. 237.
[87] M.F. Thorpe, Continuous deformations in random networks, J. Non-Cryst. Solids 57 (1983) 355–370.